

Review

Flow Control Methods and Their Applicability in Low-Reynolds-Number Centrifugal Compressors—A Review

Jonna Tiainen * , Aki Grönman , Ahti Jaatinen-Värri  and Jari Backman 

Laboratory of Fluid Dynamics, School of Energy Systems, Lappeenranta University of Technology, P.O. Box 20, 53851 Lappeenranta, Finland; aki.gronman@lut.fi (A.G.); ahti.jaatinen-varri@lut.fi (A.J.-V.); jari.backman@lut.fi (J.B.)

* Correspondence: jonna.tiainen@lut.fi; Tel.: +358-50-436-5835

Academic Editor: Reinhard Niehuis

Received: 4 September 2017; Accepted: 27 December 2017; Published: 29 December 2017

Abstract: The decrease in the performance of centrifugal compressors operating at low Reynolds numbers (e.g., unmanned aerial vehicles at high altitudes or small turbomachines) can reach 10% due to increased friction. The purposes of this review are to represent the state-of-the-art of the active and passive flow control methods used to improve performance and/or widen the operating range in numerous engineering applications, and to investigate their applicability in low-Reynolds-number centrifugal compressors. The applicable method should increase performance by reducing drag, increasing blade loading, or reducing tip leakage. Based on the aerodynamic and structural demands, passive methods like riblets, squealers, winglets and grooves could be beneficial; however, the drawbacks of these approaches are that their performance depends on the operating conditions and the effect might be negative at higher Reynolds numbers. The flow control method, which would reduce the boundary layer thickness and reduce wake, could have a beneficial impact on the performance of a low-Reynolds-number compressor in the entire operating range, but none of the methods represented in this review fully fulfil this objective.

Keywords: boundary layer; efficiency; separation

1. Introduction

At a low Reynolds number, e.g., those that are common in unmanned aerial vehicles (UAVs) at high altitudes or small turbomachines, the losses due to increased friction resulting from thicker boundary layers play a significant role. The reduction in performance due to low Reynolds numbers can be estimated using correction equations [1–4], and can be as high as 10%. In Figure 1, a schematic view of a change in compressor efficiency with a varying Reynolds number is presented. Below a lower critical chord Reynolds number ($Re_{cr,l} = wc/\nu = 200,000$), efficiency decreases rapidly without an effect of roughness whereas above an upper critical chord Reynolds number $Re_{cr,u}$, the increase in Reynolds number no longer results in increased efficiency [5].

In addition to increased friction, the performance of small turbomachines suffers from relatively larger surface roughness, blade thickness, and tip clearance. Because the surface roughness is limited by the machining process and the relative tip clearance is limited due to manufacturing tolerances and bearing technology, this review concentrates on decreasing friction losses using flow control. Researchers have tried to improve aerodynamic performance by applying various methods at different applications; for example, in axial and radial turbomachines, air vehicles and wind turbines. However, selecting an applicable method for reducing losses in low-Reynolds-number centrifugal compressors is not as straightforward since the flow field is complex and varies with different operating conditions.

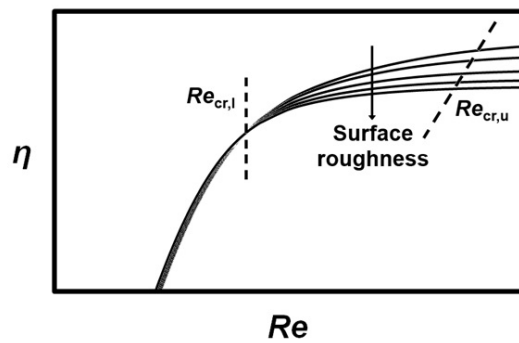


Figure 1. Schematic view of a change in compressor efficiency with a varying Reynolds number.

The complexity of the flow field arises, e.g., from the flow separation near the centrifugal compressor leading edge. In centrifugal impellers, the secondary flow transfers low-energy fluid from boundary layer and feeds it into the wake. Centrifugal forces and the channel curvature strengthen the phenomenon by preventing the turbulent mixing of the wake and main flow regions. At the radial part of the impeller where the meridional curvature does not affect the flow anymore, the forces due to the impeller rotation still maintain the wake/jet structure, and the transport of low-energy fluid from the boundary layer keeping the boundary layers separated [6].

The purposes of this review are to describe state-of-the-art flow control methods and discuss their benefits and drawbacks when applied in centrifugal compressors designed for low Reynolds numbers. Both high-altitude and small-scale machines, are accounted for in this review, as the loss generation mechanisms are similar in both and, therefore, the same methods are fundamentally applicable. The references cited in this review are mainly published from 2007 onwards. However, the investigation of a flow control method has been continuous for more than 10 years, thus earlier papers are included in this review to give a wider perspective of the research topic and to highlight its history.

Even though this review is focused on centrifugal compressors, the methods designed for both axial and radial turbomachines are examined as a means of establishing if radial machines could benefit from the knowledge gained in studies regarding axial machines, which mainly differ from the radial ones due to centrifugal effects. As a result of this review, the effects of different flow control methods are evaluated in terms of the compressor operating range and performance. In addition, conclusions are drawn about their applicability in low-Reynolds-number centrifugal compressors.

2. Classification of the Flow Control Devices

Flow control methods can be divided into active and passive methods depending on whether they require additional energy or not. To classify the methods presented in this review, the classification system used by Wood [7] and Johnson et al. [8] is utilised. Wood [7] used the following five layer system of flow control methods to classify the actuators used in unmanned aerial vehicles:

1. Does the control require the addition of energy; i.e., is it active (A) or passive (P)?
2. Does the actuator move external geometry or add/subtract external fluid; i.e., is it geometric (G) or fluidic (F)?
3. Does the actuator operate unsteadily; i.e., is it steady (S) or unsteady (U)?
4. Is the goal of the actuator to attach (AT) or to separate (SE) the flow?
5. Does the actuator change lift (L), drag (D), or both lift and drag (LD)?

The categories are listed in Table 1. Later, Johnson et al. [8] modified the classification for categorising the actuators used in wind turbines (Table 2) as follows:

- Second layer: Geometric/Fluidic (GF) actuators use mechanical motion, which is not in contact with the external flow to generate motion of air into the external flow.

- Second layer: Plasma (PI) actuators generate a body force through the use of an electric field to modify external flow.
- Third layer: Actuators that can operate both steadily and unsteadily are categorised as steady/unsteady (SU) actuators.
- Fifth layer: Actuators, the goal of which is not to change lift and/or drag but to delay stall (DS).

Johnson et al. [8] also used one layer to describe the location of the actuator according to whether it was near the leading edge (LE), at mid-chord (MC), or near the trailing edge (TE).

Table 1. Actuator classification used by Wood [7] for actuators in unmanned aerial vehicles.

Layer						
1	(A)	Active	(P)	Passive		
2	(G)	Geometric	(F)	Fluidic		
3	(S)	Steady	(U)	Unsteady		
4	(AT)	Attached	(SE)	Separated		
5	(L)	Lift	(D)	Drag	(LD)	Lift and Drag

Table 2. Additional categories in actuator classification used by Johnson et al. [8].

Layer						
1						
2	(GF)	Geometric/Fluidic	(PI)	Plasma		
3	(SU)	Steady/Unsteady				
4						
5	(DS)	Delay stall				
N	(LE)	Leading edge	(MC)	Mid-chord	(TE)	Trailing edge

To categorise the flow control methods investigated in this review, only the first three layers of the classification system of Wood [7] and Johnson et al. [8] are used. First, they are divided into active (A) and passive (P) devices. The devices utilising active methods are discussed first and a discussion of the passive methods follows. They are further divided into geometric- (G), fluidic- (F), geometric/fluidic- (GF) and plasma- (PI) based devices. The final classification is based on the operation in steady (S), unsteady (U) or in both steady and unsteady (SU) modes. These classes are presented in subsection titles describing the flow control methods. In addition to these three layers, the type of study is specified as experimental (E), numerical (N), or both experimental and numerical (EN) in the tables, in which most recent references are summarised. The methods are not classified based on the goal or use, because this review aims to introduce different goals and uses of the methods without generalisation, as one method can have several goals and/or uses.

3. Active Methods

Flow control methods based on active control require additional energy input and a control device, which enables the activation and deactivation of the flow control. Therefore, active methods can be used only when they are needed, and will not create additional losses when they are not needed, e.g., at high Reynolds numbers.

The purpose of the actuators is to reduce or eliminate flow separation [9], reduce turbulent drag [10] and/or reduce noise [11]. Low-pressure turbines (LPTs) in particular are exposed to flow separation due to increased blade loading. The increased blade loading results from the current design trend, which aims to minimise the manufacturing and maintenance costs by decreasing the number of blades.

The operation of the actuators can be steady and/or unsteady. For actuators using periodic excitation (pulsed, unsteady operation), the excitation parameters, i.e., frequency, amplitude, and duty

cycle, are important [12]. The operation of the actuators is based on introducing additional momentum in the near-wall flow [10,13]. The momentum addition is evaluated using the momentum coefficient, which is the ratio of additional momentum to the main flow momentum. The actuators using the periodic excitation are effective in the momentum coefficient range of 0.01–3% [13].

Tables 3–5 present the actuator investigations from 2004 to date. They show that drag and total pressure losses can effectively be reduced, but according to Quadrio and Ricco [14], the maximum net energy saving is only 7.3% for the actuator which could reduce drag by 44.7% due to the energy used to control the actuator. In addition to the required energy input, actuators introduce additional weight and complexity into the controlled system [10]. For example, the configuration of a pulsating jet [12] is highly complicated, and therefore, it is used mainly in the wings of air vehicles that have a long chord length.

As Tables 3–5 show, the most recently investigated active flow control devices are plasma actuators, synthetic jets, and vortex generator jets. Therefore, they are discussed in more detail below.

3.1. Plasma Actuator (Classification: Active, Plasma, Steady/Unsteady)

The purpose of a plasma actuator is to trigger transition and induce reattachment in separated flows by shifting high momentum fluid from the free-stream flow to the boundary layer. Plasma actuator research has been mainly concentrated on low-pressure turbine sections of gas turbines (Table 3), in which laminar separation is likely to occur due to low Reynolds numbers. On an airfoil of an aircraft, the plasma actuators can control flow separation during take-off and landing, whereas during cruise conditions, they can reduce skin-friction, resulting in fuel cost savings [15].

Moreau [15] provided a thorough review of the use of plasma actuators for separation control in air vehicles. For the readers' convenience, a summary of the review is given here. There are two main types of plasma actuators: The surface corona discharge (SCDA) and surface dielectric barrier discharge (SDBDA) actuators. Research on SCDA started in the 1950s. In the SCDA, high-voltage direct current (DC) is applied to two flush-mounted wires. A corona is formed around the thinner wire creating an electric wind. This electric wind accelerates the airflow tangentially to the wall, resulting in a modified boundary layer [15].

The advantage of SDBDA in reducing drag and boundary layer thickness was identified by Roth et al. [16] in 1998. In a SDBDA, two electrodes with a width of a few mm are asymmetrically separated by a dielectric layer (Teflon, Kapton, glass, ceramics, or Plexiglas) of a thickness ranging from 0.1 to a few mm, so that the upper electrode is located upstream and the lower electrode is located downstream [15]. To the flow-exposed electrode, high-voltage alternating current (AC) (from several to tens of kV) with frequencies from one to tens of kHz is applied [17,18] and another electrode is grounded (Figure 2). High voltage of a high frequency weakly ionises the surrounding fluid, producing plasma [18,19].

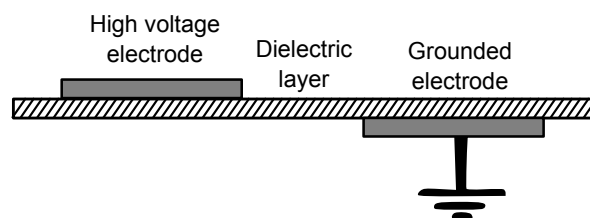


Figure 2. Schematic view of a dielectric barrier discharge plasma actuator.

Table 3. Representative summary of plasma actuator investigations.

Ref.	Year	Application	Reynolds Number	Advantage(s)
[20]	2017	LPT	17,000	Max 68% reduction in total pressure loss, eliminated separation
[21]	2017	LPT		Induced reattachment
[22]	2016	Compressor stator		Max 14% reduction in total pressure loss
[23]	2016	Gas turbines	840,000	Reduced corner vortices, 16% reduction in total pressure loss
[24]	2016	Air vehicles	2,000,000	Max 8.98% increase in lift coefficient
[25]	2015			Max 33.1% reduction in drag and 104.2% increase in lift-to-drag ratio at high AoA
[26]	2015		63,000	Induced reattachment
[27]	2015		4000; 16,000	Induced reattachment
[28]	2014	UAV	284,000	Max 2.5% increase in lift coefficient and 80% increase in lift-to-drag ratio
[17]	2013	LPT	50,000–140,000	Max 33% reduction in drag
[29]	2013	Supersonic flow		Max 5.5% reduction in normal shock wave strength
[30]	2012	LPT	17,000	Max 55% reduction in total pressure loss
[19]	2011	LPT	50,000	Induced reattachment
[31]	2011		217,000; 307,000	Control of plasma actuator
[32]	2010	Air vehicles	130,000–400,000	Induced reattachment, parameterisation of the controller
[11]	2010	Air vehicles	170,000; 340,000	Max 3.8 dB reduction in noise
[33]	2010	AC	133,800–312,200	Max 13.8% reduction in total pressure loss at 70% α
[33]	2010	AC	133,800–312,200	Max 28% reduction in total pressure loss at 70% α
[34]	2010	Air vehicles	240,000	Increased lift
[35]	2010		3000–20,000	Leading edge separation control
[36]	2009	Air vehicles	260,000	Increased lift and reduced drag
[36]	2009	Air vehicles	260,000	Increased performance compared to the steady actuation
[37]	2009		15,000	Max 32% reduction in drag, suppressed vortex shedding
[38]	2009	AC	120,000	Max 2.5% reduction in total pressure loss
[39]	2009	Air vehicles	80,000–300,000	Prevented separation only at Reynolds numbers < 100,000
[40]	2008	Jet nozzle exhaust		Enhanced jet spreading, reduced jet core length, increased turbulent kinetic energy
[41]	2007	LPT	25,000	Max 81% reduction in wake total pressure loss
[42]	2006	LPT	4500–7000	Induced reattachment
[43]	2006	LPT	10,000–100,000	Induced reattachment
[44]	2006	LPT		Induced reattachment
Outcome:				Controlled separation, induced reattachment

LPT: Low-Pressure Turbine, UAV: Unmanned Aerial Vehicle, AC: Axial Compressor, AoA: Angle of Attack.

Table 4. Representative summary of synthetic jet investigations.

Ref.	Year	Type	Application	Reynolds Number	Advantage(s)
[45]	2017	Piezoelectric diaphragms	Air vehicles	125,000	Induced reattachment
[46]	2016	Speakers		47,000	Max 5% reduction in drag, controlled vortices
[47]	2016	Piezoelectric diaphragms			Separation control
[48]	2016	Synthetic jet	UAV		Increased lift-to-drag ratio
[49]	2016	Synthetic jet	AC	840,000	Max 15.8% reduction in total pressure loss, reduced corner separation
[23]	2016	Synthetic jet	Gas turbines	840,000	Reduced corner vortices, 17% reduction in total pressure loss
[50]	2016	Synthetic jet	UAV	2,128,000	Controlled vortices
[51]	2015	Synthetic jet		896,000	Max 15% reduction in drag and 73% increase in lift, eliminated separation
[51]	2015	Synthetic jet		840,000	Max 20.32% reduction in total pressure loss, reduced secondary flow
[52]	2014	Speakers	Wind turbine	550,000	Increased lift
[53]	2014	Piezoelectric diaphragms	Wind turbine	230,000	Eliminated separation
[54]	2013	Piezoelectric diaphragms	UAV	100,000	Induced reattachment, max. 66% reduction in drag
[55]	2010	Acoustic perturbations			Max 35% increase in plenum pressure
[56]	2010	Piezofluidic actuator	Wind turbine	70,000–800,000	5–15% increase in efficiency, doubled maximum lift
Outcome:					Controlled separation, induced reattachment

Table 5. Representative summary of vortex generator jet investigations.

Ref.	Year	Type	Application	Reynolds Number	Advantage(s)
[57]	2017	Microjet	Wind turbine	1,000,000	Increased pressure coefficient
[57]	2017	Microjet	Wind turbine	1,000,000	Increased lift
[58]	2017	VGJ	Low-pressure turbine	50,000–300,000	Max 75% reduction in total pressure loss
[9]	2016	VGJ, deflected TE	Low pressure turbine	20,000; 50,000	12.5% reduction in solidity
[23]	2016	VGJ, steady	Gas turbines	840,000	Reduced corner vortices, 14% reduction in total pressure loss
[59]	2014	Microjet	Wind turbine	1,000,000	Increased lift
[60]	2013	Microjet	Low pressure turbine	50,000	Max 85% reduction in wake-loss coefficient
[12]	2013	Pulsating jet	Stemme S10 motor glider	1,750,000	30% increase in lift-to-drag ratio
[61]	2012	VGJ, unsteady	Low pressure turbine	25,000; 50,000	Separation control
[62]	2011	VGJ, unsteady	Low pressure turbine		Induced reattachment
[63]	2011	VGJ, unsteady	Low pressure turbine	25,000; 50,000	Separation control, increased lift, reduced total pressure loss
[64]	2009	VGJ, unsteady	Airfoil SS	7700 (Re_{θ})	Delayed separation
[65]	2004	VGJ, steady	Low pressure turbine	25,000	Max 50% reduction in total pressure loss
[65]	2004	VGJ, unsteady	Low pressure turbine	25,000	Max 40–50% reduction in total pressure loss
Outcome:					Controlled separation, induced reattachment

Nowadays, the SDBDAs are used more than the SCDAAs since they provide more stable discharge [15], and AC operation results in lower voltage requirement [18] and low power consumption (order of watts) [66]. On the other hand, the SDBDA may suffer from high peaks of electric input power under certain conditions; however, this may be reduced by using inductive filters between the power supply and the actuator [15].

The progress in research has resulted in new actuator designs. In 2013, Wang et al. [67] published a review of these latest designs. New designs include plasma synthetic jet actuators, plasma spark jet actuators, three-dimensional plasma actuators, and plasma vortex generators. Plasma synthetic jet actuators consist of an exposed electrode, embedded electrode and dielectric sheet. The fluid is ingested towards the actuator and ejected as a jet to the main flow. The advantage of the plasma synthetic jet actuators is acceptable power consumption (order of 100 W) [66]. The experimental results of Neretti et al. [68] indicated that the annular plasma synthetic jet actuator exhibits better performance than the linear version.

The plasma spark jet actuator consists of three electrodes. Plasma discharged into a small cavity due to an energy deposition increases the temperature and pressure of the fluid. The high-pressure fluid is ejected as a jet from the cavity to the main flow. The plasma spark jet actuator is based on arc discharges with high power consumption (order of kilowatts) [66]. The plasma spark jet with a ram-air inlet was developed by Zhou et al. [69] to overcome the limited working frequency due to the low refill rate of the cavity. The three-dimensional plasma actuator and plasma vortex generator causes vortices to re-energise the boundary layer. The three-dimensional plasma actuator consists of electrodes which have a gap between each other. Plasma vortex generators include either asymmetric (co-rotating vortices) or symmetric (counter-rotating vortices) rows of plasma actuators [67].

A thorough review of the physics of single-dielectric barrier discharge (SDBD) plasma actuators was provided by Corke et al. [18]. The benefits of plasma actuators are low power requirement, light and simple configuration (no moving parts, cavities or holes), no mechanical vibrations and fast dynamic response. At the same time, the plasma actuator requires power. The pulsed plasma actuator has proven to be more effective than the steady one [36,41,44] and it uses less power than the continuous actuator. In a pulsed operating condition in which the voltage is cycled on and off, the duty cycle depends on the flow separation state [33] varying between 5% [33] and 60% [36] in comparison to the steady actuator.

Recent research on plasma actuators has concentrated on the application of low-pressure turbines (LPTs) (Table 3), in which the plasma actuators have proven their applicability in separation control, resulting in lift augmentation and loss reduction. Plasma actuators have also shown potential in jet mixing [40], lift augmentation of air vehicle wings [32,34], suppressing vortex shedding over blunt bodies [29,37], suppressing endwall secondary flows in compressor cascades [38], reducing noise [11], and heat transfer augmentation [70]. Benard et al. [32] presented a parameterisation of the plasma actuator controller, but this discussion is beyond the topic of this review.

As the plasma actuators are used to trigger transition and induce reattachment, their applicability in centrifugal compressors is poor since the separation near the centrifugal compressor leading edge occurs due to centrifugal force and cannot be eliminated by energising the boundary layer.

3.2. Synthetic Jet (Classification: Active, Geometric/Fluidic, Unsteady)

Synthetic jets use mechanical motion (e.g., oscillating diaphragm) to inject low-momentum fluid into a cavity and eject it as a high-momentum jet to the main flow (Figure 3). Therefore, they are also referred to as Zero-Mass-Flux [56] or Zero-Mass-Blowing [13] jets. They are long and narrow spanwise slots that are located perpendicular to the airfoil surface [52]. The experimental results of Stalnov et al. [56] indicated that synthetic jets could replace passive vortex generators. The advantages of synthetic jets compared to passive vortex generators include lower drag and adjustability. In addition, their energy requirements, cost and weight are low [56]. However, the actuator requires space inside an airfoil.

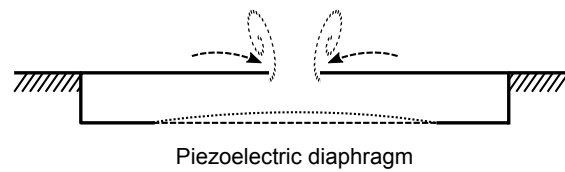


Figure 3. Schematic view of a synthetic jet with piezoelectric diaphragm.

The most recent research to concentrate on synthetic jets is presented in Table 4. As Table 4 shows, synthetic jets have effectively been used at low-Reynolds-number applications ($Re < 1,000,000$) when laminar boundary layer separation occurs and when Mach number is less than 0.1. However, a recent numerical study conducted by Xu and Zhou [50] indicated effective control of vortices when placed on the leading edge of UAV at high Reynolds and Mach numbers (2,128,000 and 0.6). To give another example of numerical studies regarding synthetic jets, Im et al. [71] and Li et al. [72] presented computational methods to reduce the computational cost of modelling synthetic jets, but these discussions are beyond the topic of this review.

Like plasma actuators, synthetic jets have poor applicability in both high-altitude and small-scale centrifugal compressors as they are based on boundary layer energising, which does not reattach the flow separated due to centrifugal force. In addition, they are effective to eliminate laminar boundary layer separation, which does not occur in centrifugal compressors. In addition, they require space for a cavity inside a blade, which practically limits their use to small turbomachinery due to material strength limitations.

3.3. Vortex Generator Jet (Classification: Active, Fluidic, Steady/Unsteady)

Vortex generator jets (Figure 4) differ from synthetic jets in that they inject additional mass flow into the main flow from a compressed air supply [12]. They are used, e.g., in combustors [73]. The injected mass flow entrains high-momentum flow from the main flow into the boundary layer reducing boundary layer separation. The most important design parameters of vortex generator jets are injected mass flow rate, jet location and pulsating frequency [74]. Vortex generator jets operating in unsteady (pulsed) operating conditions are more efficient than steady ones due to the reduced injected mass flow rate [62,65]. Kostas et al. [64] found that a counter-rotating configuration for a vortex generator jet (which consists of two jets pointing to opposite directions and results in counter-rotating streamwise vortices into the boundary layer) is more effective than a co-rotating one (which consists of individual jets pointing to same direction and results in co-rotating streamwise vortices), since it requires less injected mass flow. The unsteady vortex generator jets increase skin friction making the boundary layer less prone to separation [64].

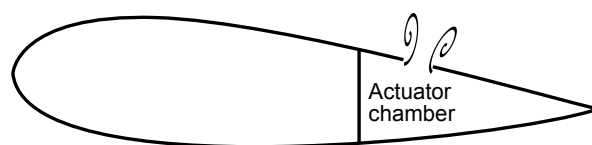


Figure 4. Simplified schematic view of a vortex generator jet.

The pulsating frequency yielding to a Strouhal number fc/U_∞ of unity is recommended [65,75]. The recommendation of the Strouhal number of unity results from the flow instabilities which are of the same order of magnitude regardless of the airfoil span [75]. As a thorough review of periodic excitation provided by Greenblatt and Wygnanski [13] pays particular attention to optimum frequencies, they are not further discussed here. The effectiveness of the unsteady vortex generator jets has shown to be independent of the duty cycle down to 1% [65]. However, the increase in wall shear stress is dependent on the injected flow rate [64].

Like plasma actuators and synthetic jets, vortex generator jets are based on boundary layer energising, which does not reattach the separated flow due to centrifugal force. In addition, the requirement for compressed air makes the use of the vortex generator jet in a low-Reynolds-number centrifugal compressor challenging. On the one hand, hot air from the compressor outlet would lower the efficiency when recirculated to the impeller. On the other hand, the implementation of these methods would result in a complex system, which is not optimal in low-Reynolds-number applications in which size and weight are important. In addition, the holes for mass flow injection (hole diameter ranging from 0.5% [61] to 2% [9] of the chord length) are vulnerable to fouling [8].

3.4. Geometric Actuators (Classification: Active/Passive, Geometric, Steady/Unsteady)

The above-mentioned active flow control methods including different actuator types are not valid in small-sized applications such as micro air vehicles or mini unmanned aerial vehicles because of the weight, volume and power consumption of the actuator [75]. A review of Gursul et al. [75] presented wing oscillation methods for increasing lift and delaying stall in low-Reynolds-number flows.

The presented flow control methods were as follows:

1. Rigid airfoils
 - (a) Deflected trailing edge vortices for pre-stall angles of attack (deflected jets)
 - (b) Convected leading edge vortices for post-stall angles of attack
2. Oscillating flexible airfoils induce reattachment by energising near-wall vortices and entraining momentum from the free-stream flow [75]
3. Self-exited flexible airfoils: Membrane airfoils (light-weight, ability to change shape), shape memory alloys [76]

Macro-fiber composite actuators are used for active flow control in unmanned aerial vehicles [77,78]. Bilgen et al. investigated experimentally piezo-based benders (Figure 5) on a NACA (National Advisory Committee for Aeronautics) 0010 airfoil profile with [78] and without [77] variable camber, camber variation being 0.25–4.35% in the trailing section. In the case of centrifugal compressor, the design parameter is blade angle distribution instead of camber and the blade angle at the blade leading edge being the most important parameter. Therefore, the camber variation in the trailing section of a NACA profile is not relevant when compared to the centrifugal compressor blade. The results indicated an increase in lift coefficient of 18.4% and 27.5% for an airfoil with and without variable camber, respectively, due to reduced separation. In addition, Phan et al. [79] investigated numerically similarly deformable compressor stator blades. Their results indicated that laminar separation could be prevented by an adaptive blade.

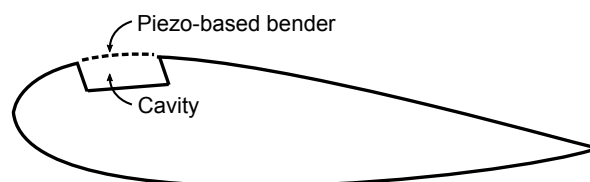


Figure 5. Example of geometric actuator using piezo-based bender.

The idea of using deformable blades to increase blade loading in a centrifugal compressor is interesting due to their lightweight and lack of power requirement. However, their applicability and advantage in centrifugal compressors should be investigated. The drawback of deformable blades in a centrifugal compressor might be the strength requirement, at least in small-scale machines operating at high rotational speeds.

4. Passive Methods

Passive flow control methods do not require additional energy. They are geometrical devices that cannot be switched on and off like the active control devices, and they affect the flow field whether they are required or not. Passive methods dominate flow control attempts due to the high cost-to-benefit ratio of active methods [74]. The advantages of passive flow control methods include lift augmentation, drag reduction, reduced tip leakage flow and separation control. However, the drawback of passive methods is that they cause additional losses when they are not required. A number of methods have been investigated in the past, but the most recently investigated approaches were selected for this review and are discussed in detail in the following subsections.

4.1. Gurney Flaps (Classification: Passive, Geometric)

Gurney flaps were first used in race cars to increase down force. A Gurney flap is a short flat plate mounted at the trailing edge perpendicular to the chord line on the pressure side of the blade, as indicated in Figure 6 [80]. The recommended flap height is less than the local boundary layer thickness [35,80] and as shown in Table 6, the studied flap sizes vary from 0.5% to 30% of the chord length. The flap increases lift by increasing pressure difference across the blade. The flap also produces a long wake, which can delay or eliminate the flow separation at the trailing edge of the suction surface. Gurney flaps have also been used for vibration control purposes. They can be implemented together with a plasma actuator at the airfoil leading edge [35], or the plasma actuator can be implemented at the Gurney flap [81]. In addition to these, Gurney flaps have been used together with dimples [82], or with a trailing edge flap [83]. The most recent review of the Gurney flap was published by Wang et al. [80].

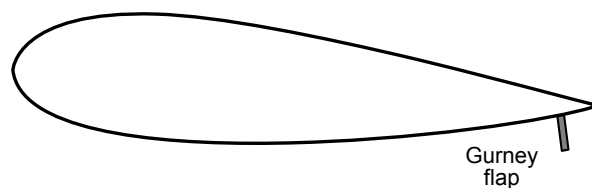


Figure 6. Gurney flap at the trailing edge on the blade pressure side.

The Gurney flap has been found to increase both lift and drag [84,85] and tip leakage [84]. With low Reynolds numbers when the separation occurs, the Gurney flaps decrease losses, but as the Reynolds number increases, the losses due to Gurney flap increase as well.

Measurements also show that the effect of a Gurney flap on lift coefficient is strongly dependent on an airfoil shape [86]. According to Cole et al. [86], the lift of aft-loaded airfoils or airfoils with a large separation region (20–30% of the suction surface) does not increase significantly or even decrease when a Gurney flap is added. The perforation of the Gurney flap has not been found to have any major impact on its efficiency either [83].

Table 6. Representative summary of Gurney flap investigations.

Ref.	Year	Type	Application	Size	Reynolds Number	Advantage(s)
[57]	2017	Microtab	Wind turbine	2% <i>c</i>	1,000,000	Increased pressure coefficient
[57]	2017	Microtab	Wind turbine	2% <i>c</i>	1,000,000	No effect on lift due to 3D effects
[87]	2017	Gurney flap		2% <i>c</i>	50,000–200,000	Better lift augmentation at higher <i>Re</i>
[82]	2015	Gurney flap		2% <i>c</i>	255,000; 360,000	35–40% increase in tangential force
[84]	2015	Gurney flap	Axial pump	0.7–1.4% <i>c</i>	690,000	25% increase in pump head, widened operating range, decreased efficiency
[59]	2014	Microtab	Wind turbine	0.5–1.2% <i>c</i>	1,000,000	Increased lift and drag
[88]	2014	Gurney flap		2% <i>c</i>	1,000,000	Lift augmentation, vibration control
[86]	2013	Gurney flap		1.04–2.38% <i>c</i>	1,000,000	Effect on max. lift coefficient depends on airfoil shape
[89]	2012	Gurney flap	Centrifugal fan	15.9% <i>b</i> ₂	30,000–82,000	Pressure ratio and operating range improved at <i>Re</i> < 69,000
[81]	2012	Gurney flap		3–7% <i>c</i>	20,000–35,000	Lift augmentation
[90]	2011	Gurney flap	Axial fan	10, 20, 30% <i>c</i>	< 100,000	Max 18% increase in efficiency with <i>q</i> _{v,max}
[83]	2011	Gurney flap		0.7–6% <i>c</i>	254,000	Lift and drag augmentation
[91]	2011	Gurney flap		1–6% <i>c</i>	105,000	Wake vortex control
[92]	2011	Gurney flap		1.5% <i>c</i>	2,100,000	Vibration reduction
[93]	2010	Jet-flap	LPT cascade		25,000–200,000	12.5% reduction in solidity
[94]	2010	Gurney flap	LPT cascade	0.5–3% <i>c</i>	25,000–200,000	12.5% reduction in solidity
[8]	2010	Microtab	Wind turbine	1–1.5% <i>c</i>	460,000	Max 37% increase in lift
[35]	2010	Gurney flap			3000–20,000	Lift augmentation
[95]	2010	Gurney flap			40,000–80,000	Lift augmentation
[96]	2003	Gurney flap	Turbine cascade	0.6–2.7% <i>c</i>	28,000–167,000	Max 9% increase in lift force
[85]	2000	Gurney flap		0.5–2% <i>c</i>	1,000,000	Increased lift and drag
Outcome:						Lift augmentation

Thamsen et al. [84] experimentally investigated the effect of Gurney flaps on the performance of an axial pump. The sizes of the studied flaps were 0.7% and 1.4% of the chord length. The results indicated that the Gurney flaps increase the head of the pump (25% at the design point, 2870 rpm, $Re = 690,000$) and widen the operational range. The head is increased due to the increased pressure difference between the pressure and suction sides of the blade. As a result of the increased pressure difference, the tip clearance flow also increases. In addition to lift, the Gurney flaps increase drag, resulting in slightly reduced efficiency.

Greenblatt [90] studied the effect of Gurney flaps on the performance of the low-Reynolds-number ($Re_c < 10^5$) axial fan. The test facility consisted of two blades of the axial fan with Gurney flaps. The studied heights of the Gurney flaps were 10%, 20% and 30% of the blade chord length. Typically the height of the Gurney flap is from 1% to 5% of the chord. In addition, thin (250 μm) and thick (1.25 mm) Gurney flaps produced from plastic were compared. Compared to thin flaps, the thick flaps better maintained their shape but added more mass to the blades. All measured flaps produced higher pressures (the maximum pressure increase was 22% at the highest flow rate) than the blades without flaps. The isentropic efficiency was decreased due to Gurney flaps at lower flow rates whereas it was increased at higher flow rates in comparison to the blades without flaps. The 10% thin Gurney flap produced the greatest increase in efficiency (the maximum efficiency increase was 18% at the highest studied flow rate).

Byerley et al. [96] used Gurney flaps on the pressure surface near the trailing edge of the turbine blade to prevent laminar separation. Laminar separation occurred on the suction surface of the turbine blade at low Reynolds numbers (based on inlet conditions and axial chord) of 28,000 and 65,000. The separation was prevented by the Gurney flaps, which turned and accelerated the flow toward the suction surface of the neighbouring blade. The size of the studied Gurney flap varied from 0.6% to 2.7% of the axial chord.

Bechert et al. [85] investigated the differences between 2D Gurney flap, divergent trailing edge and Gurney flap, where the corner regime on the pressure side of the airfoil was filled so that a quarter of a circle was formed. The authors concluded that the improvement of the filled corner was only marginal and a smaller Gurney flap is better than a larger divergent trailing edge. As a conclusion, the modifications in Gurney flap geometry reduce the mechanical stiffness of the Gurney flap and make the geometry more complicated.

In addition, active Gurney flaps (deployable flaps or miniature trailing-edge effectors) have been under investigation [88,92]. Byerley et al. [96] presented the need to retract the Gurney flap with high Reynolds numbers when separation does not occur, which would make the Gurney flap an active flow control method. Microtabs are small Gurney flaps that operate with an actuator. The advantages of microtabs include fast response, simple configuration, and low power requirements [8]. Disadvantages include noise generation, air leakage, and installation challenges due to the limited space near the airfoil trailing edge [8]. In 2010, Chen et al. [93] investigated a jet-flap, which is an aerodynamic flap generated by a jet of air near the airfoil trailing edge. A jet-flap eliminates separation by increasing momentum on the airfoil suction surface, which results in higher loading.

To conclude, Gurney flaps are not structurally complex and they have low space requirement unlike the active flow control methods. Therefore, Gurney flaps could potentially be placed at the trailing edge of the blade in centrifugal compressors near stall conditions as they delay separation near the trailing edge and increase loading, resulting in increased efficiency and widened operating range. However, the applicability of Gurney flaps in other than stall conditions is poor since they increase drag and tip leakage. Therefore, they are not recommended in low-Reynolds-number centrifugal compressors.

4.2. Riblets (Classification: Passive, Geometric)

The drag reducing riblet structures found in nature (shark skin [97] and bird beak [98]) have inspired researchers to reduce drag in engineering applications. Riblets are small streamwise aligned

grooves that shift turbulent vortices farther away from the surface resulting in decreased momentum transfer and wall shear stress [99,100]. The reduction of friction by means of riblets has been an active field of study at both the fundamental and application level, for example, Nieuwstadt et al. [101], Bechert et al. [102] and Lietmeyer et al. [103].

The drag reductions that have been reported have typically been about 5% [102,104] but reductions as high as 13% have also been reported [105]. Table 7 summarises the recent research on riblets. The strength of the pressure gradient can be determined using the Clauser parameter β . As shown in Table 7, there seems to be a disagreement as to whether riblets are also beneficial with strong adverse pressure gradients. Nieuwstadt et al. [101] drew attention to the difficulties associated with measuring the drag indirectly in the work by Truong and Pulvin [106] and Squire and Savill [107]. According to Nieuwstadt et al. [101], the momentum balance cannot predict with confidence whether the drag is increased or decreased. Use of the drag balance measurement instead of the momentum balance measurement has led to results that indicate more effective drag reduction with increasing adverse pressure gradient [101].

Table 7. Representative summary of the riblet investigations at different values of Clauser parameter β .

Ref.	Year	Application	Reynolds Number	$\beta = \frac{\delta^*}{\tau_{w0}} \frac{dp}{dx}$	Effect on Drag
[97]	2016	Transportation, medical, industry	4180	0	−11.6%
[98]	2016	Transportation, industry	4200	0	−3.9%
[108]	2015	Mild APG	860 (Re_θ)	0.5	−8%
[109]	2015	LPT	76,400		±0%
[110]	2014	Axial compressor	150,000–900,000	>0	±0%
[111]	2013	Wind turbine	2,200,000		−6%
[112]	2012	Air vehicles	1720 (Re_θ)	0	−7%
[113]	2011	Wind turbine	1,000,000–1,850,000		−4...−5%
[114]	2010	ZPG	1000 (Re_θ)	0	−4...−5%
[114]	2010	Mild APG	1000 (Re_θ)	~0.05	−7...−8%
[114]	2010	Stronger APG	1000 (Re_θ)	~0.15	−9...−10%
[104]	2002	Air vehicles	250,000–3,900,000	0–0.1	−5...−8%
[104]	2002	Air vehicles	250,000–3,900,000	0.2–2.2	−8%
[105]	1996	APG	–	2.2	−13%
[101]	1993	ZPG	~800,000–2,250,000	0	−5%
[101]	1993	APG	~800,000–2,250,000	0.4–1.5	−4%...−7%
[107]	1989	ZPG, air vehicles	34,000,000	0	−5.5%
[107]	1989	APG, air vehicles	34,000,000	0.5	±0%
[106]	1989	APG	10,000–500,000	−0.1...0.1	–
[106]	1989	APG	10,000–500,000	>0.2	±0%
Mean value:					−7%

APG: Adverse Pressure Gradient; ZPG: Zero Pressure Gradient.

The drag reduction performance of riblets is higher at low Reynolds numbers than at high Reynolds numbers [115,116] and ice, fouling, and wearing weakens the drag reduction capability of riblets [10].

The design of the riblets, that is, shape, spacing, positioning and angle, plays a major role in the achievable drag reduction. For example, Sareen et al. [113] tested four different v-shaped (sawtooth) riblets on a wind turbine airfoil and found that the location of the riblet film, the Reynolds number, and the angle of attack influenced the performance of riblets. A drag reduction of 4–5% was found with optimal riblets placed in the turbulent region, whereas non-optimal riblets produced up to 10–12% drag increase.

Chamorro et al. [111] found that v-type grooves produced the best performance on a wind turbine airfoil, roughly 6% maximum drag reduction in the expected operational range. According to Bechert et al. [102], a trapezoidal riblet shape has a better drag reduction than a v-type riblet shape. Recently, trapezoidal riblets have been used on axial compressor blades because they represent the best compromise between drag reduction and structural strength [117]. A recent review of the drag

reduction performance of riblets, which was written by Dean and Bhushan [118], concluded that the blade-shaped riblets provide the optimum drag reduction; however, due to their fragile nature, trapezoidal or scalloped riblets are recommended. In addition, the recent research shows that the blade-shaped riblets produce the best drag reduction [97]. Examples of the riblet shapes are shown in Figure 7.

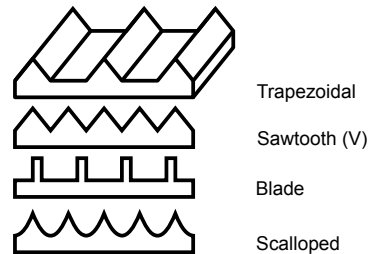


Figure 7. Shapes of riblets.

The optimal size of the riblet can be evaluated in terms of the dimensionless riblet spacing:

$$s^+ = \frac{su_\tau}{\nu}, \quad (1)$$

where s is the riblet spacing, $u_\tau = \sqrt{\tau_w/\rho}$ the friction velocity, and ν the kinematic viscosity. Values of the dimensionless riblet spacing s^+ in the range of 15–17 have been suggested [99,117]. The riblet spacing must be small enough ($s^+ < 30$), or otherwise one streamwise vortex would fit into one groove between the riblets resulting in increased drag [102]. The optimal ratio between riblet height and spacing of $h/s = 0.5$ was suggested by Bechert et al. [102].

In addition to the dimensionless riblet spacing s^+ , the dimensionless wall distance y^+ can be used as an optimisation parameter. García-Mayoral and Jiménez [119] suggested that the breakdown of riblet performance is associated with spanwise quasi-two-dimensional vortices below $y^+ \approx 30$.

Positioning of the riblets also plays a major role in drag reduction. Lietmeyer et al. [117] suggested that the riblet geometry should be adapted locally to the flow conditions because high riblets near the blade leading edge increase friction due to earlier transition resulting from a roughness effect. Drag reduction potential outside the separation region was pointed out by Lietmeyer et al. [117], but was not investigated.

The fourth design parameter is the angle of the riblet. The experimental results of Lietmeyer et al. [117] suggested the use of riblet tip that is as sharp as possible. A riblet angle of 30° or even 45° is technologically feasible according to Bechert et al. [102]. The sharp riblet tip plays an important role in the effectiveness of the riblet; e.g., experimental and numerical studies of Miao et al. [109] indicated that the aerodynamic performance advantage gained from the weakened passage vortex is cancelled out by the additional friction and mixing losses due to riblet surface quality at the turbine endwall.

For manufacturing riblets, grinding [103], laser-structuring [103], vinyl riblet films [120], and nanoparticle-reinforced paints [121] have been used.

The drag reduction potential of riblets could be utilised in centrifugal compressors if the riblets can be manufactured in the streamwise direction. The manufacturing of riblets could be feasible on shroud and/or hub surfaces of the impeller and diffuser but their drag reduction capability might be changed to drag increase at off-design conditions when the flow conditions vary from the design point.

As it was said in the beginning of Section 4.2, the riblets are small streamwise aligned grooves. In Section 5.2, grooves are discussed, but here the difference between the riblets and grooves is highlighted for the readers' convenience. The grooves (Section 5.2) at the shroud surface have shown potential in modifying tip leakage flow, resulting in more uniform flow field. However, these grooves are not aligned in streamwise direction like riblets and they are larger than riblets.

Therefore, the increased wetted surface due to the grooves results in increased drag, whereas, in the case of riblets, the vortices do not fit in the small “grooves” between the riblet tips, but are shifted farther away from the surface, resulting in decreased drag.

The potential effect of riblets on centrifugal compressor efficiency can roughly be estimated based on their drag reduction potential. As the drag reduction is proportional to friction factor reduction, the increase in efficiency can be estimated based on the decrease in friction factor using the efficiency correction equation published by Dietmann and Casey [4]. If the maximum drag reduction of 13% [105] is assumed, the efficiency improvement varies in the range of 1–3% with a decreasing Reynolds number being greater below a lower critical chord Reynolds number of 200,000.

4.3. Squealers and Winglets (Classification: Passive, Geometric)

In addition to friction losses, tip leakage losses are higher in micro-scale low-Reynolds-number compressors than in larger compressors. Higher tip leakage losses result from relatively larger tip clearance in micro-scale compressors due to the manufacturing tolerances.

Squealers and winglets can be used to weaken tip leakage flow and they have been investigated separately and in conjunction in the literature (Table 8). Squealers are vertical protrusions on a blade tip that point towards a casing. If squealers are applied on both the pressure and suction sides of the blade tip, a cavity is formed between them. Winglets are horizontal protrusions on a blade tip pointing towards adjacent blades. Schematics of squealer and winglet geometries are shown in Figure 8. They can be applied on pressure, suction, or both sides of the blade, separately or together, and they do not have to cover the whole blade length.

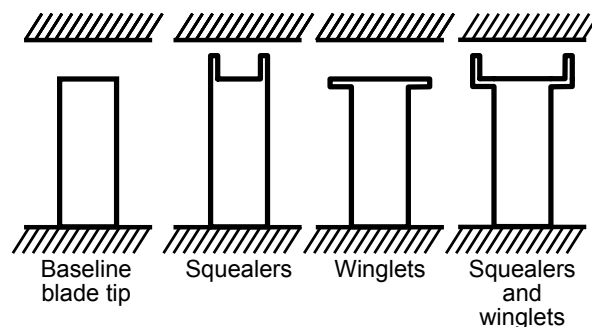


Figure 8. Schematic view of squealer and winglet geometries.

The purpose of the squealers and winglets is to reduce the losses associated with tip leakage flow. The following principles for tip leakage flow control have been published:

1. Splitting the loading due to the tip leakage between the pressure and suction side squealers reduces losses [122].
2. Thin squealers prevent the fluid from reattaching to their tip surface [122].
3. Winglets weaken the passage vortex [123].
4. Winglets decrease the pressure difference over the blade tip [122].
5. Pressure side winglet weakens tip leakage [124].
6. Pressure side squealer strengthens tip leakage [125].

Different configurations of squealers have been under investigation since they can be applied on pressure, suction, or both pressure and suction sides separately or together with winglets. If the width of the winglets is so large that the winglets of adjacent blades touch each other, they form a partial shroud. Sometimes, ribs between the squealers are used. However, they have not shown any significant benefits in aerodynamic performance [126]. Numerical studies have found that openings in squealers on the blade suction side at the leading and trailing edges can be beneficial [127]. Due to the openings, the cavity vortex is strengthened and sealing effectiveness is improved [127]. Among several

squealer and winglet geometries, Schabowski and Hodson [122] found the geometry with pressure and suction side squealers and winglets to provide the best total pressure loss reduction in a turbine cascade. Further optimisation of the geometry led to a geometry with squealers implemented on both pressure and suction sides, but the suction side squealer was on the top of the suction side winglet and the suction side leading edge was open [128].

In a high-pressure turbine, the tip leakage flow is pushed farther away from the blade suction side by the winglet, resulting in reduced interaction between the passage and tip leakage vortices and losses [127]. With increasing winglet width-to-pitch ratio (w/p), the tip leakage vortex stretches less towards the mid-span and the total pressure loss increases for $w/p \leq 2.64\%$, decreases for $2.64\% < w/p < 10.55\%$, and then becomes nearly constant [123].

The effect of squealers on aerodynamic performance is connected to the operating conditions of a centrifugal compressor (improved performance at high flow rates, decreased performance at low flow rates) [126]. Increase in squealer cavity depth reduces performance [126], while the increase in squealer cavity width improves it [126]. The study conducted by Da Soghe et al. [126] indicated that the best efficiency gain was achieved with the squealer depth of 15% of the blade thickness and with the squealer width of 80% of the blade thickness. The study of Li et al. [129] indicated that the best efficiency gain is achieved with the squealer depth of three times the tip clearance (1.38 mm) when the squealer is as wide as possible.

Ma et al. [130] experimentally investigated the effect of suction-side squealer tip geometry on the performance of an axial compressor. They studied the tip leakage vortex behaviour using PIV and a statistical approach, and concluded that the squealer increased the static pressure rise but, at the same time, the tip leakage vortex was stronger and there was more reversed flow than in the baseline case. However, the leakage vortex dissipated faster behind the trailing edge with the squealer. The squealer geometry also caused a larger blockage in the blade passage. Thus, it could be assumed that the squealer geometry studied in the paper of Ma et al. would increase losses in micro-scale centrifugal compressor if it increased blockage and strengthened the tip leakage flow.

To conclude, the use of squealers and winglets with optimised geometry could be beneficial for small-scale compressor performance since they reduce tip leakage by decreasing pressure difference over the blade tip. In small-scale machines, the tip leakage losses increase due to relatively larger tip clearances. However, the effectiveness of the squealers depends on the compressor operating conditions; i.e., their performance is better at high flow rates than at low flow rates. In a small-scale centrifugal compressor, the squealer depth of 15% of the blade thickness would roughly mean approximately 0.05 mm and the width of 80% of the blade thickness would mean 0.28 mm (with a lower limit for blade thickness of 0.35 mm [131]).

Table 8. Representative summary of squealer and winglet investigations.

Ref.	Year	Type	Application	Reynolds Number	Tip Leakage	Maximum Effect on		
						Efficiency	Operating Range	Total Pressure Loss
[132]	2017	Squealer and winglet	Turbine cascade		reduced			−8.5%
[133]	2017	Squealer and winglet	HPT	1,200,000	reduced	+0.9%		
[127]	2016	Squealer and winglet	HPT blade		reduced	heat transfer augmentation		
[126]	2016	Squealers with ribs	CC		reduced	+ at high q_v		
[126]	2016	Squealer	CC		reduced	+0.47%		
[124]	2016	Winglet	NASA 37		reduced	−0.27%	+33.74%	
[124]	2016	Winglet	NASA 37		increased	−0.47%	−9.29%	
[125]	2016	Squealer	HPT blade		increased	−1.177%pt		
[125]	2016	Squealer	HPT blade		reduced	−0.047%pt		
[125]	2016	Squealer	HPT blade		reduced	−0.459%pt		
[125]	2016	Squealer with pressure side opening	HPT blade		reduced	−0.883%pt		
[125]	2016	Squealer with suction side opening	HPT blade		reduced	−0.341%pt		
[134]	2016	Squealer	Turbine cascade	209,000	reduced			−4%
[129]	2016	Squealer	PW-E3 HPT blade		reduced	+0.33%		
[135]	2016	Winglet	HPT cascade	650,000	−33.6%			−28%
[135]	2016	Winglet with seals	HPT cascade	650,000	−88.7%			−50%
[136]	2016	Winglet	HPT cascade	650,000	−1.32%			−11.36%
[136]	2016	Partial shroud	HPT cascade	650,000	−16.53%			−20.89%
[137]	2016	Squealer and winglet	HPT blade	160,000	reduced	9.4% lower entropy generation		
[123]	2015	Squealer and winglet	Turbine cascade	209,000	reduced			−5.8%
[130]	2015	Squealer	AC	750,000		±0%		
[138]	2014	Winglet	Compressor cascade	430,000	reduced			+
[138]	2014	Winglet	Compressor cascade	430,000				− (slightly)
[139]	2014	Squealer	Turbine cascade	209,000	reduced			−11.6%
[140]	2014	Squealer	HPT blade	1,540,000	reduced			
[128]	2014	Squealer and winglet	Turbine cascade	440,000	reduced			−29%
[122]	2014	Squealer and winglet	Turbine cascade	440,000	reduced			−17%
[141]	2012	Winglet	Turbine cascade	209,000	reduced			−1.4%
[141]	2012	Winglet	Turbine cascade	209,000	reduced			−1.7%
[142]	2008	Squealer	Turbine cascade	209,000	reduced			−16%
Mean value:						+0.2%	+12%	−16%

HPT: High-Pressure Turbine; CC: Centrifugal Compressor, AC: Axial Compressor.

4.4. Turbulence and Vortex Generators (Classification: Passive, Geometric)

Passive vortex generators have been investigated recently in wind turbine applications [143–147] where the flow separation reduces power at start-up and low wind speeds [87]. In addition to the wind turbines, they have been investigated in centrifugal compressors [148], tractor-trailers [149] and aeroplanes [150]. As the active vortex generator jets, passive vortex generators are used for separation control. In this review, dimples [65] and tripping devices (tapes) [148] are grouped into vortex generators.

Streamwise vortices generated by the vortex generators entrain high-momentum fluid into the boundary layer resulting in eliminated or delayed separation [143] or induced reattachment [151]. Similarly, the vortex generators affect the interaction between shock waves and boundary layers resulting in the reduction of shock-induced separation [152]. The effects of vortex generators on shock waves have been thoroughly reviewed by Panaras and Lu [152].

A number of different vortex generator configurations have been studied, and reported in the literature (Table 9). At zero and adverse pressure gradient flows, joined and spaced vortex generator vanes, respectively, are effective [74].

To delay the separation, the vortex generators should be placed close to the natural separation point [146,153,154]. The vortex generators have been shown to delay the dynamic stall of wind turbines if placed at the leading edge [145], to weaken the secondary flow in compressor cascade passage if placed at the endwall [74], and to induce reattachment if placed on the suction side of the compressor blade [74,155].

In addition to vortex generator location, the device height and spacing are important design parameters [87,154]. A thorough review of low-profile vortex generators (with a device height from 10% to 50% of the boundary layer thickness) was provided by Lin [154]. Lin investigated a wide range of low-profile vortex generators and concluded that the vane-type generators (Figure 9) are the most effective at reducing the separation region. Tay et al. [156] investigated dimples and concluded that drag reduction could be enhanced by increasing the dimple depth from 1.5% to 5% of its diameter, but increased dimple depth can result in increased flow separation causing additional drag. Therefore, deeper dimples are more suitable at higher Reynolds numbers.

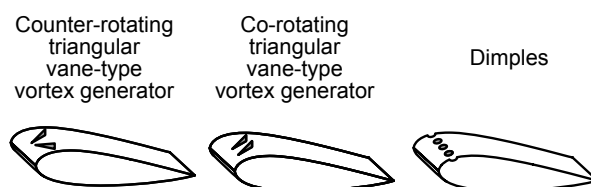


Figure 9. Examples of vortex generators and dimples on an airfoil suction side.

Whereas the low-profile vortex generators should be located close to the separation point, Rivir et al. [65] stated that dimples could effectively reduce separation and losses even when located after the separation point [65]. However, the dimples are most effective when located upstream of the separation point [65]. Dimples (Figure 9) are affordable, robust, retrofittable, and manufacturable [65]. Despite the advantages of dimples, with exception of the investigations of Zhao et al. [155] and Ismail and Vijayaraghavan [82], they have not recently been employed in turbomachinery applications. Zhao et al. [155] found that dimples located at 30–60% of the chord length reduced the total pressure losses more than dimples located closer to the trailing edge. Their results indicated that the dimples either reduced the losses or had no significant impact; however, they did not increase the losses in the investigated incidence angle range of $-5.3 \dots +10^\circ$. Heat transfer augmentation by the dimples [157–160] has been investigated more than their aerodynamic performance.

At low Reynolds numbers, wishbone type low-profile vortex generators are used on an airfoil [154]. If vortex generators with the height, h , between 10% and 50% of the boundary layer thickness are

placed less than $100h$ upstream of the separation point, the size of the separation bubble is reduced resulting in a thinner turbulent boundary layer and reduced drag. On the other hand, at a small angle of attack (6°), no significant lift augmentation or drag reduction on NACA 0012 airfoil has been found [153].

Dimples are not as prone to fouling and wearing as riblets [10]; however, they cause additional drag [74]. The smaller the vortex generator, the lower the additional drag, but at low Reynolds numbers, a small vortex generator might not be sufficient to induce reattachment [74].

To conclude, the use of vortex generators in a centrifugal compressor would require information about the separation point. As the ability of vortex generators to increase lift is based on induced reattachment, their applicability in an impeller of a centrifugal compressor is poor since the separation in a centrifugal compressor is caused by centrifugal force. The use of vortex generators in diffuser vanes might be an option, but the location of the separation point varies depending on the operating point.

4.5. Miscellaneous Passive Methods

Numerous additional flow control methods other than those already discussed have been investigated in the literature. This review is limited to those that have been investigated recently and are applicable in engineering applications.

By decreasing the incidence angle at the impeller blade leading edge, positive preswirl widens the compressor operating range [161]. Whitfield and Abdullah [161] used the variable inlet volute geometry with a rectangular cross-section to generate a positive preswirl. Because straight uncambered inlet guide vanes provide only zero incidence, aligned uncambered inlet guide vanes are inefficient due to large incidence angles and wakes, and cambered inlet guide vanes cannot be oriented to provide zero incidence.

Galindo et al. [162] showed both experimentally and numerically that the negative preswirl generated by radial guide vanes can also decrease the incidence angle. Galindo et al. used the negative preswirl to overcome the non-uniformity of the flow field at the impeller inlet of the turbocharger. The non-uniform flow field was a consequence of the 90° bend near the impeller inlet. The incidence angle was reduced less with the negative preswirl than with the positive one, but in addition to a reduced incidence angle, the negative preswirl increased the pressure ratio, unlike the positive one. On the other hand, the efficiency was reduced due to negative preswirl.

The numerical results of Guendogdu et al. [163] showed that the number of compressor stator vanes can be reduced when jet flaps with Coanda surfaces (a curved surface near the trailing edge) are used, because the Coanda surface near the stator vane trailing edge increases the diffusion factor and maintains the exit flow angle of the reference case with more stator vanes and without Coanda surface. A passive Coanda surface has also been implemented together with an active jet flap stator, namely the vortex generator jet (Figure 10), which shifts the separation point on the suction surface closer to the trailing edge and decreases the size of the trailing edge wake. Thus, the velocity gradient and total losses near the trailing edge are reduced.

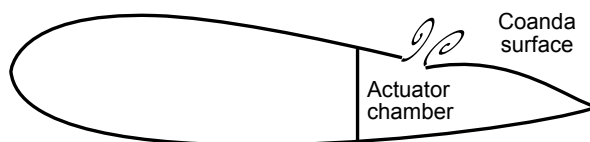


Figure 10. Schematic view of a blade with vortex generator jet and Coanda surface.

Table 9. Representative summary of vortex generator investigations.

Ref.	Year	Type	Application	Reynolds Number	Advantage(s)
[87]	2017	Vane type	Wind turbine	50,000–200,000	Better lift augmentation at low Re , eliminated separation
[157]	2017	Dimples	Gas turbine	25,000	Heat transfer augmentation
[143]	2017	Array of orifices	Wind turbine	700,000–1,100,000	Max 14% increase in maximum lift coefficient
[143]	2017	Array of orifices	Wind turbine	270,000–1,300,000	Max 9% increase in maximum lift coefficient
[74]	2017	Rib-type	AC	170,000	Induced reattachment, strengthened secondary flow at the endwalls if placed over full span
[74]	2017	Vane type	AC	170,000	Increased pressure coefficient and weakened secondary flow at the endwall
[145]	2016	Vane type	Wind turbine	50,000	Delayed dynamic stall
[164]	2016	Vane type	Air vehicles	200,000	Max 21% increase in maximum lift coefficient, decreased lift-to-drag ratio
[149]	2016	Vane type	1:20 scale tractor-trailer	530,000	Max 12.9% decrease in wake vortex size
[146]	2016	Rod type	Wind turbine	1,000,000	Max 11% increase in lift-to-drag ratio
[10]	2016	Dimples		40,000	Max 4% decrease in drag
[151]	2016	Rod type	Helicopter rotor blades		Induced reattachment
[155]	2016	Dimples	AC	489,000	Max 20% decrease in total pressure loss
[165]	2016	Dimples	Gas turbine	8200–50,500	30–80% increase in friction factor, increased turbulence kinetic energy
[147]	2015	Vane type	Wind turbine	870,000	Max 44% increase in lift
[156]	2015	Dimples		5,000–35,000	Max 3% decrease in drag
[166]	2012	Dimples	Air vehicles	494,000	Length of the attached boundary layer increased max. 371%
[148]	2012	Tripping tape	CC		Increased operating range
[160]	2010	Dimples	Gas turbine	1,060,000	10–20% increase in heat transfer coefficient
[153]	2008	Wing lip type, oscillating	Turbomachinery, air vehicles	100,000	Eliminated separation
[153]	2008	Wing lip type	Turbomachinery, air vehicles	100,000	Partially eliminated separation
[65]	2004	Dimples	LPT	25,000	Max 45–50% reduction in total pressure loss
Outcome:					Separation control, lift augmentation

Shahpar et al. [167] numerically investigated the use of a profiled endwall to increase the performance of a turbine. They found that a profiled endwall affects more leakage flow in the hub side rim seal than secondary flows in the blade passage resulting in the maximum improvement in efficiency of 0.43%. Zaryankin et al. [168] showed experimentally and numerically that streamwise fins on the stator vane passage endwall of a turbine reduce the total energy loss coefficient by around 12%.

In centrifugal compressors, the vortex generator jet with a Coanda surface could theoretically be beneficial in an impeller but the implementation of the vortex generator jet is not practically possible. However, the vortex generator jet might be replaced with a slot in the impeller blade, but as it should be located at the point of separation, it is beneficial only at one operating point.

5. Active and Passive Casing Treatments (Classification: Active, Fluidic, Steady/Unsteady and Passive, Geometric, Steady)

Active and passive casing treatments consist of flow control methods applied in turbomachinery casing, and have been developed to improve performance, increase stall margin, and enhance stability close to the stall [169]. Table 10 presents an overview of the studies on active and passive casing treatments that were conducted from 2003 onwards. Applications vary from axial (AC) and centrifugal (CC) compressors to high pressure turbine (HPT) cascade and channel flows. The advantages of the investigations are presented as a maximum reported effect on machine efficiency, pressure ratio, operating range and/or surge margin.

Active casing treatments mean fluidic devices operating in steady or unsteady conditions. The high-momentum fluid is injected into the main flow to energise low-momentum fluid, and additional energy is used to inject the fluid. Passive casing treatments either recirculate fluid from higher pressure to lower pressure (e.g., from the compressor outlet to inlet) through recirculation slots or shift low-momentum fluid through grooves.

5.1. Injection, Suction, and Recirculation

A self-circulating casing treatment is a passive casing treatment in which the high-momentum fluid is recirculated from higher to lower pressure. In the past, the stall margin was improved by casing treatment; however, this reduced efficiency. Recently, the investigations have shown that, with the proper selection of casing treatment parameters, both the stall margin and the performance can be improved [170]. The most important design parameters for a self-circulating casing treatment are the width and position of the bleed slot [171–173], recirculation flow rate [172] and casing porosity [174].

Irsch et al. [175] found that, in the case of a turbine blade, the optimum position for the injection tube is slightly on the blade pressure side at the trailing edge. The injection results in the reduced strength of the vortex oscillations, smaller vortices, and reduced total pressure loss. In an axial compressor, the optimum location for the injection is at the rotor blade leading edge, or upstream of it [170,176] and an injector throat height lower than four times the rotor tip clearance is recommended [170]. In this optimum location, the injection acts on the tip leakage flow delaying the onset of stall.

In a centrifugal compressor, air is generally recirculated from the impeller or the volute to the inlet of the impeller. Wang et al. [177] located the bleed holes near the separation point and the injection nozzle at the impeller inlet, whereas Skoch [178] injected air into the vaneless space between the impeller and diffuser. The flow direction can also be radial in the bleed port, and air is injected far upstream of the impeller inlet. The numerical results of Tun and Sakaguchi [172] indicated that the optimum location for the bleed hole is near the splitter blade leading edge. Figure 11 presents an example of a self-circulating casing treatment in a centrifugal compressor. High-momentum fluid is recirculated from the impeller to the impeller inlet through the recirculation slot.

Table 10. Representative summary of active and passive casing treatments.

Ref.	Year	Type	Application	Reynolds Number	Mass Flow Ratio	Maximum Effect on			
						Efficiency	Pressure Ratio	Operating Range	Surge Margin
[179]	2017	Injection hole	Axial fan	120,000–240,000	2.6–6.0%		+		
[180]	2017	Recirculating slots	CC			–	+	+	
[180]	2017	Bleed slots	CC		40%	±0%	+10%	+	
[181]	2017	Axial slots	MC			–0.7%			+26.4%
[182]	2017	Recirculating slots	AC		0.27–0.38%	±0%	+		+20%
[183]	2017	Injection nozzle	CC		0–80%		–1%	+3%	+40%
[184]	2017	Injection nozzle	AC						+
[185]	2017	Grooves	HPT cascade	220,000			Max 4% reduction in total pressure loss		
[186]	2017	Injection nozzle	HPT cascade	60,000	0.4%		20% reduction in total pressure loss		
[187]	2016	Grooves	AC			±0%	±0%		
[188]	2016	Grooves	Channel flow	2648–30,000			40% reduction in drag		
[171]	2016	Recirculating slots with vanes	CC, Ns = 1.00		up to 20%	–0.25%pt		+25%	+69%
[171]	2016	Recirculating slots with vanes	CC, Ns = 0.85		up to 20%	–0.4%pt		+30%	+94%
[189]	2016	Recirculating slots	AC		0.47%	±0%			+6.12%
[190]	2016	Grooves	AC						+5.7%
[191]	2016	Bleed chamber	AC			±0%	±0%		+3.5...+9.3%
[172]	2016	Recirculating slots	CC		–0.15...+0.15%	+			+
[170]	2016	Recirculating slots	AC		7.4–8.4%	+2%			+10%
[174]	2016	Recirculating slots	AC			–2.71%			+33.05%
[169]	2015	Grooves	CC			±0%	+2.48%		+
[192]	2015	Injection nozzle	CC		1.5%				+37%
[193]	2015	Injection nozzle	CC		1–12%				+30%
[175]	2015	Injection tube	Turbine blade	323,955	0.3–4%	Reduction in total pressure loss			
[194]	2015	Recirculating slots	AC			–	–		+5.7%
[195]	2013	Recirculating holes	CC			–1%	–2%		+10%
[196]	2013	Recirculating slots	CC		11%	±0%			+20%
[197]	2013	Recirculating slots	CC			–1%		+17%	
[197]	2013	Recirculating slots with vanes	CC			+2%	+4%	+	
[198]	2012	Recirculating slots	CC		up to 13%		±0%	+	
[198]	2012	Recirculating slots with vanes	CC		up to 17%		±0%	+	
[173]	2012	Recirculating slots	CC						+
[199]	2011	Recirculating holes	CC		–2...+6%	–0.7%	+0.2%		+30%
[177]	2010	Recirculating slots	CC		4.9%	+0.2...+1.5%		+20%	
[200]	2012	Injection nozzle	CC		2–11%	±0%		+20%	
[176]	2007	Injection nozzle	AC		0.15%				+9%
[176]	2007	Injection nozzle	CC		0.9%			+10%	
[201]	2005	Injection nozzle	CC		0.9–4.6%		±0%	±0%	
[202]	2004	Injection nozzle	CC		0.5%			+25%	
[178]	2003	Injection nozzle	CC		0.9%		–1%		+15%
[178]	2003	Bleed control tube	CC				–5.5%		+56%
Mean value:					7.9%	±0%	–0.4%	+19%	+26%

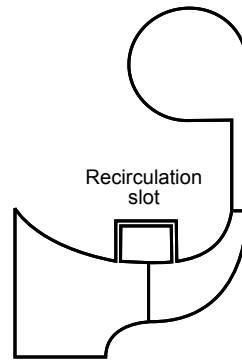


Figure 11. Example of a self-circulating casing treatment in a centrifugal compressor.

Nie et al. [176] achieved a 10% increase in surge margin by implementing the injection in the impeller inducer. Figure 12 shows a schematic view of the injection nozzle in the impeller inducer, where the high-momentum fluid is circulated from, e.g., the compressor outlet. Hirano et al. [200] proposed that the optimum circumferential position for a single injector is on the opposite side of the volute tongue. For double injection, the optimum circumferential position for the first injection is between the volute tongue and the location at 30° to the rotational direction when the second injection is located at 135° from the tongue against the rotational direction, resulting in a 30% increase in surge margin [193]. The increase in surge margin was related to reduced reversed flow in the diffuser close to surge [193]. According to Zheng et al. [173], the non-symmetric casing treatment around the shroud periphery improves the surge margin more than a symmetric casing treatment (surge flow rate being 10% lower with the non-symmetric casing treatment) due to the reduced circumferential flow distortion at the impeller inlet.

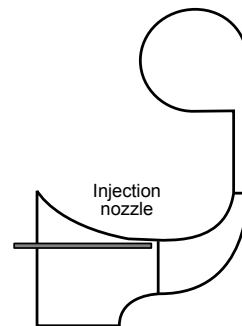


Figure 12. Schematic view of an injection nozzle in a centrifugal compressor.

The injection of air from the compressor outlet to the hub in the vaneless space between the impeller and vaned diffuser has not provided any notable improvement in compressor performance [201]. The best configuration (tubes of 10 mm in diameter and immersed from the shroud to a depth of 50% of the diffuser height) for the compressor stabilisation in the vaneless space between the impeller and the vaned diffuser improved the surge margin by 56%, but the pressure ratio was reduced by 5.5% [178]. The lowest reduction in pressure ratio (-1%) was achieved by injecting air through nozzles in the streamwise direction, resulting in a 15% increase in surge margin.

In the vaneless space, the injection increases mass flow rate, resulting in increased radial velocity component and decreased absolute flow angle (α from the radial direction), which, in turn, prevents recirculation. Thus, the stable operating range is widened. The injection also increases blockage and decreases diffusion, in the vaneless space, resulting in a reduced pressure ratio [178,203]. Injection through the shroud surface recovers part of the operating range lost by the leakage flow through the labyrinth seal [203].

Instead of injecting through the shroud surface, Skoch [178] recommended stabilising the compressor with the tubes located on the shroud surface. The tubes bleed low-momentum flow from the vaneless space and decrease the flow area, resulting in an increased radial velocity component and a decreased absolute flow angle (α from the radial direction) at the diffuser vane leading edge, which prevents recirculation.

Jung and Pelton [171] found that the greatest increase in the operating range and lowest reduction in efficiency is achieved with a slot area of 23% of the centrifugal compressor inlet area. If the bleed slot is shifted downstream from the impeller inducer, the compressor operating range increases but efficiency decreases [171]. For a casing porosity, Wang et al. [170] found the optimum value of 25%.

Both injection and suction are commonly used control methods in diffusers [204], but they do not significantly improve the performance of the unstalled diffuser.

In the literature, the reported recirculation flow rate through the recirculation slot of a self-circulating casing treatment varied from 0.15% [176] to an extremely high 80% [183] of the main mass flow rate in the literature. Zhu et al. [174] distinguished a linear correlation between the injection mass flow rate and stall margin improvement from numerical results.

Injection configuration is complex and increases the weight of the system due to, e.g., high-speed valves for air injection. Kern et al. [184] managed to increase the injection mass flow rate by decreasing the injected primary mass flow rate while also utilising the ejector effect. Primary mass flow was injected from the high-pressure compressor, and it entrained an ambient secondary mass flow rate.

To conclude, the bleed-recirculation casing treatment with different bleed port and injection nozzle locations shifts the surge line to lower flow rates but it has a complex structure. In addition, injection configuration is complex and increases the weight of the system due to, e.g., high-speed valves for air injection. Therefore, the injection, suction or recirculation casing treatments could be beneficial for separation/stall control and surge margin improvement in larger compressors, but their applicability in small-scale machines is poor due to the space requirements. Furthermore, they do not reduce friction losses in low-Reynolds-number compressors.

5.2. Grooves

Circumferential grooves at the shroud surface (Figure 13) reduce the boundary layer thickness near the grooves. The grooves transfer low momentum fluid from the pressure to the suction side while energising it by decreasing the radial velocity and increasing the tangential velocity. From 4 to 8 grooves should be located near the separation point with a spacing of one-half groove width. It is recommended that the groove depth and width are approximately of the order of the boundary layer displacement thickness [205].

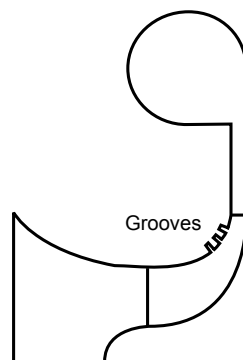


Figure 13. Schematic view of grooves at the centrifugal compressor shroud surface.

Barei et al. [169] experimentally and numerically studied the effect circumferential grooves at the shroud wall near the impeller trailing edge on the centrifugal compressor ($d_2 = 90$ mm) had on performance. They studied the difference between the smooth casing and casing with 2, 3 or 4 grooves,

respectively. The first three grooves from the trailing edge were close to each other, but the fourth was a bit more upstream. The results showed that the case with four grooves increased the pressure ratio but efficiency remained the same. The authors believed that the increased pressure ratio was caused by the grooves which increased the blade loading upstream of the groove. Because the first, second and third grooves were so close to each other, the loading could not be increased between them as much as upstream from the third and fourth grooves. Therefore, the authors speculated as to whether the first and second grooves near the impeller trailing edge were required at all. The efficiency was not improved due to additional friction losses because of the increased wall surface in the grooves.

In addition to increased blade loading, the grooves shifted the tip leakage flow further away from the blade suction side resulting in more uniform flow field at the impeller outlet. In addition, the wake was weakened and its size was reduced by the grooves. However, these mechanisms could not improve the efficiency, but balanced the additional friction losses.

Du [181] compared circumferential grooves and axial slots in a mixed-flow compressor. Axial slots delay stall more effectively than circumferential grooves but at a higher efficiency loss. The optimum location of the circumferential grooves is in the middle of the tip chord. According to Du [181], the axial slot can be optimised to produce a 26.4% improvement in surge margin with only 0.7% reduction in efficiency. However, the optimum parameters of a slot configuration depend on the compressor type.

Cevik et al. [187] implemented grooves at the endwall of an axial compressor rotor to reduce the extent to which the compressor performance was sensitive to tip clearance size. Grooves did not enhance the performance but they decreased tip leakage over two adjacent blades and reduced performance and stall margin sensitivity to the changing tip clearance. The grooves investigated were sawtooth-shaped circumferential grooves with a depth of the tip clearance size.

Overall, grooves could be beneficial in low-Reynolds-number centrifugal compressors in which they increase the pressure-ratio and weaken the wake. Micro-scale compressors with relatively large tip clearances, in particular, could benefit from the modified tip leakage flow and more uniform flow field at the impeller outlet. However, the drawback of the grooves is that the increased wall surface results in additional friction losses so that the efficiency cannot be improved.

6. Theoretical Applicability in Low-Reynolds-Number Centrifugal Compressors

This paper presented a review of the active and passive flow control methods that have been used in numerous engineering applications. Table 11 presents a summary of the reviewed flow control methods, their purposes and working principles. The purposes are also illustrated in Figure 14. Most of the methods described in this paper are applicable to drag reduction and separation control. The riblets reduce drag by decreasing wall shear stress, whereas the drag/total pressure loss reduction of plasma actuators and synthetic jets results from separation control.

The methods that are developed for separation control tend to trigger transition and induce reattachment of separated laminar flow. In centrifugal compressors, the separation in the impeller occurs due to centrifugal force. Therefore, the separation control methods that are based on boundary layer energising do not lead to reattachment in the impeller. In principle, the separation control could be beneficial, e.g., by passive turbulence and vortex generators in diffuser vanes, but the location of separation point varies depending on the operating point making the design difficult.

Boundary layer separation has also been prevented on low-Reynolds-number unmanned aerial vehicle airfoils through the use of geometric actuators such as piezo-based benders, which allow the airfoil to oscillate. Membrane airfoils, which allow the airfoil to change shape, could be an interesting research subject in centrifugal compressors, but in small-scale compressors that operate at high rotational speeds, their applicability would be limited due to structural demand.

Table 11. Purpose of flow control methods.

Type	Purpose	Principle
Plasma actuator	Separation control	Induced reattachment by energising boundary layer
Synthetic jet	Separation control	Induced reattachment by energising boundary layer
Vortex generator jet	Separation control	Induced reattachment by energising boundary layer
Geometric actuators	Lift augmentation, stall delay	Induced reattachment by energising boundary layer
Gurney flaps	Lift augmentation	Improved pressure difference across the airfoil when mounted at the trailing edge
Riblets	Drag reduction	Decreased momentum transfer to the surface
Squealers and Winglets	Tip leakage control	Decreased pressure difference over the blade tip
Turbulence and vortex generators	Separation control, lift augmentation	Energised boundary layer
Casing treatment: injection, suction, recirculation	Separation/Stall control	Increased mass flow rate
Casing treatment: grooves	Surge margin improvement	Changed tip leakage vortex trajectory

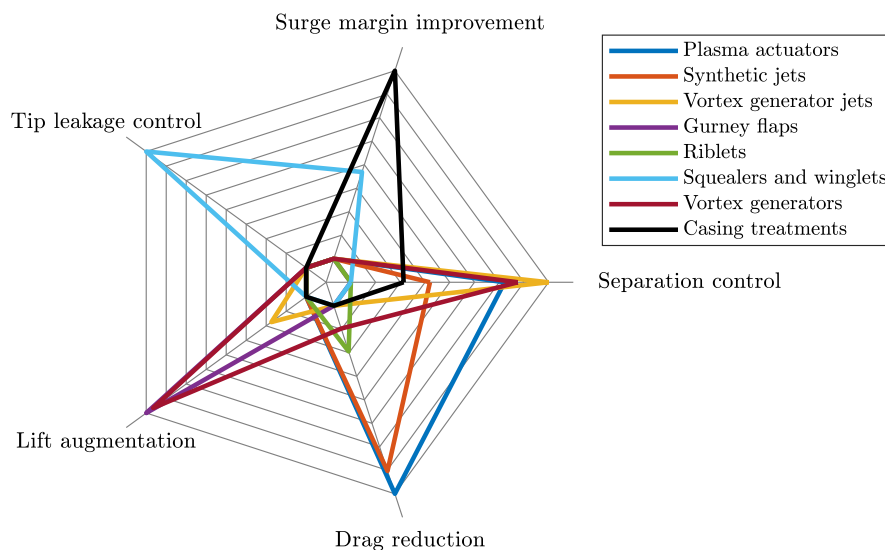


Figure 14. Quantitative presentation of the flow control method purposes.

Instead of separation control, the drag reduction and blade loading improvement would be more beneficial for improving the performance of low-Reynolds-number centrifugal compressors as the efficiency of low-Reynolds-number machines might be even 10% lower than that of high-Reynolds-number machines. Therefore, Gurney flaps could be potentially placed at the trailing edge of the blade in centrifugal compressors near stall conditions as they delay separation near the trailing edge and increase loading, resulting in increased efficiency and widened operating range. However, Gurney flaps are not recommended in low-Reynolds-number centrifugal compressors as they increase drag and tip leakage at other than stall conditions.

The drag reduction potential of riblets could be utilised in centrifugal compressors if the riblets can be manufactured in the streamwise direction. The manufacturing of riblets could be feasible on the shroud and/or hub surfaces of the impeller and diffuser but their drag reduction capability would be changed to drag increase at off-design conditions when the flow conditions vary from the design point.

In addition to increased friction losses in low-Reynolds-number compressors, relatively large tip clearances increase losses in small-scale machines. The losses associated with the tip clearance could be tackled with squealers and winglets. However, the effectiveness of the squealers depends on the compressor operating conditions; i.e., their performance is better at high flow rates than at low flow rates.

A restriction for using a complex flow control system in a small-scale machine is the additional weight of the control device. It is challenging to set a maximum weight allowable for the control device, as it depends on the application. A low-Reynolds-number centrifugal compressor can be a part of various applications, e.g., unmanned aerial vehicles, refrigeration systems, micro-scale gas turbines for distributed energy generation, etc. When the micro-scale applications are developed, the aim is to minimize the size and weight of the system. Therefore, in this manuscript it is assumed that any additional weight due to the flow control device should be avoided.

The bleed-recirculation casing treatment with different bleed port and injection nozzle locations shifts the surge line to lower flow rates but it has a complex structure. Injection configuration is complex and increases the weight of the system due to, e.g., high-speed valves for air injection. The grooves could be beneficial in low-Reynolds-number centrifugal compressors in which they increase the pressure-ratio and weaken the wake. In particular, micro-scale compressors with relatively large tip clearances could benefit from the modified tip leakage flow and more uniform flow field at the impeller outlet.

Overall, it is important that the flow control method does not deteriorate the efficiency of the centrifugal compressor although the operating range is widened. The flow control methods that require

the actuator to be located at a fixed separation point are not applicable in centrifugal compressors, as the flow separates in the impeller due to centrifugal force and the separation point in the diffuser vanes varies depending on the operating point. The advantage of a widened operating range is low if the efficiency cannot be improved in the entire operating range of a low-Reynolds-number compressor as the passive flow control methods might deteriorate the efficiency in off-design conditions.

It would be beneficial for the low-Reynolds-number centrifugal compressor performance in the entire operating range if the size of the wake could be reduced, as the wake occurs in the blade passage at every operating condition. The wake is increased with the decreasing Reynolds number, as the secondary flows shift the low-momentum fluid from the relatively larger boundary layers to the wake. The boundary layer thickness of the baseline centrifugal compressor is approximately 1 mm, whereas in the micro-scale it is relatively 25–30% thicker but absolutely one tenth of the baseline boundary layer thickness being approximately 0.1 mm. The centrifugal compressors discussed in this review are assumed subsonic.

7. Conclusions

The aim of this review was to represent the state-of-the-art of the active and passive flow control methods used to improve performance and/or widen the operating range in numerous engineering applications. The applications include axial and radial turbomachines, air vehicles, and wind turbines. In addition, the purpose was to investigate the applicability of the flow control methods in centrifugal compressors in order to improve the compressor efficiency when operating at low Reynolds numbers.

To conclude, the selection of the flow control method depends on the application. The active methods, riblets, turbulence and vortex generators could be beneficial in a machine that mostly works close to its design point. The casing treatments and Gurney flaps would work in a machine in which the operating range needs to be widened without improving the efficiency near the design point. The use of a vortex generator jet or injection in a low-Reynolds-number centrifugal compressor is challenging as they require compressed air. On the one hand, hot air from the compressor outlet would lower the efficiency when recirculated to the impeller. On the other hand, the implementation of these methods would result in a complex system, which is not optimal in low-Reynolds-number applications in which size and weight are important.

In low-Reynolds-number centrifugal compressors, the method should increase performance by reducing drag, increasing blade loading, or reducing tip leakage whereas separation control is not a significant feature. In addition to aerodynamic demands, the flow control method cannot be structurally complex and it should meet structural demands. Based on these requirements, passive flow control methods, like riblets, squealers, winglets and grooves, could be beneficial in terms of the performance of low-Reynolds-number centrifugal compressors. The riblets with optimum geometry at the design operating point could potentially improve the compressor efficiency from 1% to 3% depending on the Reynolds number. Two studies on the squealers implemented in the centrifugal compressor indicate minor efficiency improvement ($< +0.5\%$). One study on the grooves implemented in the centrifugal compressor do not indicate any improvement in the efficiency, but they have potential in modifying the tip leakage flow. However, the drawback of passive methods is that their performance depends on the operating conditions and might be negative at higher Reynolds numbers. The flow control method, which would reduce the boundary layer thickness and result in reduced wake, would be beneficial for low-Reynolds-number compressor performance in the entire operating range, but none of the methods represented in this review fully fulfils this objective.

Acknowledgments: The authors would like to acknowledge the financial contribution of the Academy of Finland. This research is part of the “Low-Reynolds number kinetic compression” project, which was funded by the Academy of Finland under grant number 274897.

Author Contributions: J.T. reviewed the literature and was mainly responsible for writing the paper. A.G. and A.J.-V. participated in analyzing the data and also contributed to writing the manuscript. J.B. contributed funding.

Conflicts of Interest: The authors declare no conflict of interest. The founding sponsors had no role in the design of the study; in the collection, analyses, or interpretation of data; in the writing of the manuscript, and in the decision to publish the results.

Nomenclature

Latin Alphabet

b_2	blade height at the impeller outlet	[m]
w	relative velocity	[m/s]
c	chord	[m]
s	span	[m]

Greek Alphabet

ν	kinematic viscosity	[m ² /s]
-------	---------------------	---------------------

Abbreviations

HPT	High-Pressure Turbine
LPT	Low-Pressure Turbine
VGJ	Vortex Generator Jet
PS	Pressure Side
SS	Suction Side
TE	Trailing Edge
LE	Leading Edge
UAV	Unmanned Aerial Vehicle
AC	Axial Compressor
CC	Centrifugal Compressor
MC	Mixed-flow Compressor
AoA	Angle of Attack
ZPG	Zero Pressure Gradient
APG	Adverse Pressure Gradient
A	Active
P	Passive
S	Steady
U	Unsteady
AT	Attached
SE	Separated
L	Lift
D	Drag
LD	Lift and Drag
GF	Geometric/Fluidic
G	Geometric
F	Fluidic
PI	Plasma
SU	Steady/Unsteady
DS	Delay stall
MC	Mid-chord
SCDA	Surface Corona Discharge Actuator
SDBDA	Surface Dielectric Barrier Discharge Actuator

References

1. Wiesner, F.J. A New Appraisal of Reynolds Number Effects on Centrifugal Compressor Performance. *J. Eng. Gas Turbines Power* **1979**, *101*, 384–392.
2. Casey, M. The Effects of Reynolds Number on the Efficiency of Centrifugal Compressor Stages. *J. Eng. Gas Turbines Power* **1985**, *107*, 541–548.
3. Pelz, P.; Stonjek, S. The Influence of Reynolds Number and Roughness on the Efficiency of Axial and Centrifugal Fans—A Physically Based Scaling Method. *J. Eng. Gas Turbines Power* **2013**, *135*, 052601, doi:10.1115/1.4022991.
4. Dietmann, F.; Casey, M. The Effects of Reynolds Number and Roughness on Compressor Performance. In Proceedings of the 10th European Conference on Turbomachinery: Fluid Dynamics and Thermodynamics, Lappeenranta, Finland, 15–19 April 2013; pp. 532–542.
5. Casey, M.; Robinson, C. A Unified Correction Method for Reynolds Number, Size, and Roughness Effects on the Performance of Compressors. *Proc. Inst. Mech. Eng. Part A J. Power Energy* **2011**, *225*, 864–876.
6. Eckardt, D. Detailed Flow Investigations within a High-Speed Centrifugal Compressor Impeller. *J. Fluids Eng.* **1976**, *98*, 390–399.
7. Wood, R. A Discussion of Aerodynamic Control Effectors (ACEs) for Unmanned Air Vehicles (UAVs). In Proceedings of the 1st Technical Conference and Workshop on Unmanned Aerospace Vehicle, Systems, Technologies, and Operations, Portsmouth, VA, USA, 20–23 May 2002.

8. Johnson, S.; Baker, J.; Van Dam, C.; Berg, D. An Overview of Active Load Control Techniques for Wind Turbines with an Emphasis on Microtabs. *Wind Energy* **2010**, *13*, 239–253.
9. Li, C.; Yan, P.; Wang, X.; Han, W.; Wang, Q. Numerical Study of Combining Steady Vortex Generator Jets and Deflected Trailing Edge to Reduce the Blade Numbers of Low Pressure Turbine Stage. *J. Therm. Sci.* **2016**, *25*, 511–517.
10. van Nesselrooij, M.; Veldhuis, L.; van Oudheusden, B.; Schrijer, F. Drag Reduction by Means of Dimpled Surfaces in Turbulent Boundary Layers. *Exp. Fluids* **2016**, *57*, 142, doi:10.1007/s00348-016-2230-9.
11. Li, Y.; Zhang, X.; Huang, X. The Use of Plasma Actuators for Bluff Body Broadband Noise Control. *Exp. Fluids* **2010**, *49*, 367–377.
12. Grund, T.; Nitsche, W. Wind Tunnel and Flight Tests with Active Flow Control on a S10 Glider Configuration. In *New results in Numerical and Experimental Fluid Mechanics VII, Contributions to the 17th STSB/DGLR Symposium, Berlin, Germany, 9–10 November 2010*; Dillmann, A., Heller, G., Kreplin, H.-P., Nitsche, W., Peltzer, I., Eds.; Springer-Verlag: Berlin/Heidelberg, Germany, 2013; Volume 121, pp. 117–124.
13. Greenblatt, D.; Wygnanski, I.J. The Control of Flow Separation by Periodic Excitation. *Prog. Aerosp. Sci.* **2000**, *36*, 487–545.
14. Quadrio, M.; Ricco, P. Critical Assessment of Turbulent Drag Reduction through Spanwise Wall Oscillations. *J. Fluid Mech.* **2004**, *521*, 251–271.
15. Moreau, E. Airflow Control by Non-Thermal Plasma Actuators. *J. Phys. D Appl. Phys.* **2007**, *40*, 605–636.
16. Roth, J.R.; Sherman, D.M.; Wilkinson, S.P. Boundary Layer Flow Control with a One Atmosphere Uniform Glow Discharge Surface Plasma. In Proceedings of the 36th AIAA Aerospace Sciences Meeting and Exhibit, Reno, NV, USA, 12–15 January 1998.
17. Marks, C.; Sondergaard, R.; Wolff, M.; Anthony, R. Experimental Comparison of DBD Plasma Actuators for Low Reynolds Number Separation Control. *J. Turbomach.* **2013**, *135*, 011024, doi:10.1115/1.4006517.
18. Corke, T.; Enloe, C.; Wilkinson, S. Dielectric Barrier Discharge Plasma Actuators for Flow Control. *Annu. Rev. Fluid Mech.* **2010**, *42*, 505–529.
19. Burman, D.; Simon, T.; Kortshagen, U.; Ernie, D. Separation Control Using Plasma Actuators: Steady Flow in Low Pressure Turbines. In Proceedings of the ASME Turbo Expo, Vancouver, BC, Canada, 6–10 June 2011; Volume 5, pp. 1869–1878.
20. De Giorgi, M.; Ficarella, A.; Marra, F.; Pescini, E. Micro DBD Plasma Actuators for Flow Separation Control on a Low Pressure Turbine at High Altitude Flight Operating Conditions of Aircraft Engines. *Appl. Therm. Eng.* **2017**, *114*, 511–522.
21. Pescini, E.; Marra, F.; De Giorgi, M.; Francioso, L.; Ficarella, A. Investigation of the Boundary Layer Characteristics for Assessing the DBD Plasma Actuator Control of the Separated Flow at Low Reynolds Numbers. *Exp. Therm. Fluid Sci.* **2017**, *81*, 482–498.
22. De Giorgi, M.; Pescini, E.; Marra, F.; Ficarella, A. Plasma Actuator Scaling down to Improve its Energy Conversion Efficiency for Active Flow Control in Modern Turbojet Engines Compressors. *Appl. Therm. Eng.* **2016**, *106*, 334–350.
23. Traficante, S.; De Giorgi, M.; Ficarella, A. Flow Separation Control on a Compressor-Stator Cascade Using Plasma Actuators and Synthetic and Continuous Jets. *J. Aerosp. Eng.* **2016**, *29*, 04015056.
24. Zhang, X.; Huang, Y.; Wang, X.; Wang, W.; Tang, K.; Li, H. Turbulent Boundary Layer Separation Control Using Plasma Actuator at Reynolds Number 2000000. *Chin. J. Aeronaut.* **2016**, *29*, 1237–1246.
25. Liu, R.; Niu, Z.; Wang, M.; Hao, M.; Lin, Q. Aerodynamic Control of NACA 0021 Airfoil Model with Spark Discharge Plasma Synthetic Jets. *Sci. China Technol. Sci.* **2015**, *58*, 1949–1955.
26. Sato, M.; Nonomura, T.; Okada, K.; Asada, K.; Aono, H.; Yakeno, A.; Abe, Y.; Fujii, K. Mechanisms for Laminar Separated-Flow Control Using Dielectric-Barrier-Discharge Plasma Actuator at Low Reynolds Number. *Phys. Fluids* **2015**, *27*, 117101, doi:10.1063/1.4935357.
27. Yakeno, A.; Kawai, S.; Nonomura, T.; Fujii, K. Separation Control Based on Turbulence Transition Around a Two-Dimensional Hump at Different Reynolds Numbers. *Int. J. Heat Fluid Flow* **2015**, *55*, 52–64.
28. Zhang, X.; Huang, Y.; Wang, W.; Wang, X.; Li, H. Unmanned Air Vehicle Flow Separation Control Using Dielectric Barrier Discharge Plasma at High Wind Speed. *Sci. China Phys. Mech. Astron.* **2014**, *57*, 1160–1168.
29. Sun, Q.; Cheng, B.; Li, Y.; Kong, W.; Li, J.; Zhu, Y.; Jin, D. Computational and Experimental Analysis of Mach 2 Air Flow over a Blunt Body with Plasma Aerodynamic Actuation. *Sci. China Technol. Sci.* **2013**, *56*, 795–802.

30. Matsunuma, T.; Segawa, T. Effects of Input Voltage on Flow Separation Control for Low-Pressure Turbine at Low Reynolds Number by Plasma Actuators. *Int. J. Rotating Mach.* **2012**, doi:10.1155/2012/902548.
31. Corke, T.; Bowles, P.; He, C.; Matlis, E. Sensing and Control of Flow Separation Using Plasma Actuators. *Philos. Trans. R. Soc. A Math. Phys. Eng. Sci.* **2011**, *369*, 1459–1475.
32. Benard, N.; Moreau, E.; Griffin, J.; Cattafesta, L.N., III. Slope Seeking for Autonomous Lift Improvement by Plasma Surface Discharge. *Exp. Fluids* **2010**, *48*, 791–808.
33. Li, Y.H.; Wu, Y.; Zhou, M.; Su, C.B.; Zhang, X.W.; Zhu, J.Q. Control of the Corner Separation in a Compressor Cascade by Steady and Unsteady Plasma Aerodynamic Actuation. *Exp. Fluids* **2010**, *48*, 1015–1023.
34. Little, J.; Nishihara, M.; Adamovich, I.; Samimy, M. High-Lift Airfoil Trailing Edge Separation Control Using a Single Dielectric Barrier Discharge Plasma Actuator. *Exp. Fluids* **2010**, *48*, 521–537.
35. Schuele, C.; Greenblatt, D. Combined Plasma and Gurney Flap Flow Control at Low Flight Reynolds Numbers. *AIAA J.* **2010**, *48*, 2714–2718.
36. Benard, N.; Jolibois, J.; Moreau, E. Lift and Drag Performances of an Axisymmetric Airfoil Controlled by Plasma Actuator. *J. Electrostat.* **2009**, *67*, 133–139.
37. Jukes, T.; Choi, K.S. Flow Control Around a Circular Cylinder Using Pulsed Dielectric Barrier Discharge Surface Plasma. *Phys. Fluids* **2009**, *21*, 084103, doi:10.1063/1.3194307.
38. Li, G.; Xu, Y.; Lin, B.; Zhu, J.; Nie, C.; Ma, H.; Wang, Z. Control of Endwall Secondary Flow in a Compressor Cascade with Dielectric Barrier Discharge Plasma Actuation. *Sci. China Ser. E Technol. Sci.* **2009**, *52*, 3715–3721.
39. Mabe, J.; Calkins, F.; Wesley, B.; Woszidlo, R.; Taubert, L.; Wygnanski, I. Single Dielectric Barrier Discharge Plasma Actuators for Improved Airfoil Performance. *J. Aircr.* **2009**, *46*, 847–855.
40. Benard, N.; Bonnet, J.; Touchard, G.; Moreau, E. Flow Control by Dielectric Barrier Discharge Actuators: Jet Mixing Enhancement. *AIAA J.* **2008**, *46*, 2293–2305.
41. Rizzetta, D.; Visbal, M. Numerical Investigation of Plasma-Based Flow Control for Transitional Highly Loaded Low-Pressure Turbine. *AIAA J.* **2007**, *45*, 2554–2564.
42. Boxx, I.; Woods, N.; Newcamp, J.; Franke, M.; Rivir, R. A PIV Study of a Plasma Discharge Flow-Control Actuator on a Flat Plate in an Aggressive Pressure Induced Separation. In Proceedings of the ASME Turbo Expo 2006: Power for Land, Sea, and Air, Barcelona, Spain, 8–11 May 2006; Volume 3, pp. 1231–1242.
43. Huang, J.; Corke, T.; Thomas, F. Plasma Actuators for Separation Control of Low-Pressure Turbine Blades. *AIAA J.* **2006**, *44*, 51–57.
44. Huang, J.; Corke, T.; Thomas, F. Unsteady Plasma Actuators for Separation Control of Low-Pressure Turbine Blades. *AIAA J.* **2006**, *44*, 1477–1487.
45. Feero, M.; Lavoie, P.; Sullivan, P. Three-Dimensional Span Effects of High-Aspect Ratio Synthetic Jet Forcing for Separation Control on a Low Reynolds Number Airfoil. *J. Vis.* **2017**, *20*, 45–51.
46. Gao, N.; Li, Y.; Bai, H.; Wu, C. Effects of Synthetic Jets on a D-Shaped Cylinder Wake at a Subcritical Reynolds Number. *Flow Turbul. Combust.* **2016**, *97*, 729–742.
47. Kim, M.; Lee, B.; Lee, J.; Kim, C. Experimental and Computational Study on Separation Control Performance of Synthetic Jets with Circular Exit. *Int. J. Aeronaut. Space Sci.* **2016**, *17*, 296–314.
48. Lee, J.; Lee, B.; Kim, M.; Kim, C. Active Flow Control on a UCAV Planform Using Synthetic Jets. *Int. J. Aeronaut. Space Sci.* **2016**, *17*, 315–323.
49. Qin, Y.; Wang, R.; Song, Y.; Chen, F.; Liu, H. Active Flow Control on a Highly Loaded Compressor Stator Cascade with Synthetic Jets. In Proceedings of the ASME Turbo Expo 2016: Turbomachinery Technical Conference and Exposition, Seoul, South Korea, 13–17 June 2016.
50. Xu, X.; Zhou, Z. Analytical Study on the Synthetic Jet Control of Asymmetric Flow Field of Flying Wing Unmanned Aerial Vehicle. *Aerosp. Sci. Technol.* **2016**, *56*, 90–99.
51. De Giorgi, M.; De Luca, C.; Ficarella, A.; Marra, F. Comparison Between Synthetic Jets and Continuous Jets for Active Flow Control: Application on a NACA 0015 and a Compressor Stator Cascade. *Aerosp. Sci. Technol.* **2015**, *43*, 256–280.
52. De Vries, H.; Van Der Weide, E.T.A.; Hoeijmakers, H.W.M. Synthetic Jet Actuation for Load Control. *J. Phys. Conf. Ser.* **2014**, *555*, 012026, doi:10.1088/1742-6596/555/1/012026.
53. Gul, M.; Uzol, O.; Akmandor, I.S. An Experimental Study on Active Flow Control Using Synthetic Jet Actuators Over S809 Airfoil. *J. Phys. Conf. Ser.* **2014**, *524*, 012101, doi:10.1088/1742-6596/524/1/012101.
54. Goodfellow, S.; Yarusevych, S.; Sullivan, P. Momentum Coefficient as a Parameter for Aerodynamic Flow Control With Synthetic Jets. *AIAA J.* **2013**, *51*, 623–631.

55. Greenblatt, D.; Arzuan, G. Active Control of Flow Separation in a Radial Blower. *J. Fluids Eng. Trans. ASME* **2010**, *132*, 0512021–0512026.
56. Stalnov, O.; Kribus, A.; Seifert, A. Evaluation of Active Flow Control Applied to Wind Turbine Blade Section. *J. Renew. Sustain. Energy* **2010**, *2*, doi:10.1063/1.3518467.
57. Chen, H.; Qin, N. Trailing-Edge Flow Control for Wind Turbine Performance and Load Control. *Renew. Energy* **2017**, *105*, 419–435.
58. Kurz, J.; Hoeger, M.; Niehuis, R. Active Boundary Layer Control on a Highly Loaded Turbine Exit Case Profile. In Proceedings of the 12th European Conference on Turbomachinery Fluid Dynamics & Thermodynamics, Stockholm, Sweden, 3–7 April 2017.
59. Blaylock, M.; Chow, R.; Cooperman, A.; Van Dam, C. Comparison of Pneumatic Jets and Tabs for Active Aerodynamic Load Control. *Wind Energy* **2014**, *17*, 1365–1384.
60. Fernandez, E.; Kumar, R.; Alvi, F. Separation Control on a Low-Pressure Turbine Blade Using Microjets. *J. Propuls. Power* **2013**, *29*, 867–881.
61. Volino, R.; Ibrahim, M. Separation Control on High Lift Low-Pressure Turbine Airfoils Using Pulsed Vortex Generator Jets. *Appl. Therm. Eng.* **2012**, *49*, 31–40.
62. Postl, D.; Balzer, W.; Fasel, H. Control of Laminar Separation Using Pulsed Vortex Generator Jets: Direct Numerical Simulations. *J. Fluid Mech.* **2011**, *676*, 81–109.
63. Volino, R.J.; Kartuzova, O.; Ibrahim, M.B. Separation Control on a Very High Lift Low Pressure Turbine Airfoil Using Pulsed Vortex Generator Jets. *J. Turbomach.* **2011**, *133*, 041021, doi:10.1016/j.applthermaleng.2011.08.028.
64. Kostas, J.; Foucaut, J.; Stanislas, M. The Effects of Pulse Frequency and Duty Cycle on the Skin Friction Downstream of Pulsed Jet Vortex Generators in an Adverse Pressure Gradient Turbulent Boundary Layer. *Aerosp. Sci. Technol.* **2009**, *13*, 36–48.
65. Rivir, R.; Sondergaard, R.; Bons, J.; Yurchenko, N. Control of Separation in Turbine Boundary Layers. In Proceedings of the 2nd AIAA Flow Control Conference, Portland, OR, USA, 28 June–1 July 2004.
66. Zong, H.; Kotsonis, M. Effect of Slotted Exit Orifice on Performance of Plasma Synthetic Jet Actuator. *Exp. Fluids* **2017**, *58*, 17, doi:10.1007/s00348-016-2299-1.
67. Wang, J.J.; Choi, K.S.; Feng, L.H.; Jukes, T.N.; Whalley, R.D. Recent Developments in DBD Plasma Flow Control. *Prog. Aerosp. Sci.* **2013**, *62*, 52–78.
68. Neretti, G.; Seri, P.; Taglioli, M.; Shaw, A.; Iza, F.; Borghi, C. Geometry Optimization of Linear and Annular Plasma Synthetic Jet Actuators. *J. Phys. D Appl. Phys.* **2017**, *50*, 015210.
69. Zhou, Y.; Xia, Z.; Luo, Z.; Wang, L.; Deng, X. A Novel Ram-Air Plasma Synthetic Jet Actuator for Near Space High-Speed Flow Control. *Acta Astronaut.* **2017**, *133*, 95–102.
70. Li, G.; Yu, J.; Chen, F.; Liu, H.; Song, Y.; Li, L. Large Eddy Simulation of Saw Tooth Plasma Actuator for Improving Film Cooling Efficiency. *Proc. Inst. Mech. Eng. Part A J. Power Energy* **2017**, doi:10.1177/0957650917704596.
71. Im, D.; Choi, S.; McClure, J.; Park, S. Numerical Analysis of Synthetic Jet Flows Using a Diagonally Implicit Harmonic Balance Method With Preconditioning. *Comput. Fluids* **2017**, *147*, 12–24.
72. Li, W.; Jin, D.; Zhao, Y. Efficient Nonlinear Reduced-Order Modeling for Synthetic-Jet-Based Control at High Angle of Attack. *Aerosp. Sci. Technol.* **2017**, *62*, 98–107.
73. Bauer, S.; Hampel, B.; Sattelmayer, T. Operability Limits of Tubular Injectors with Vortex Generators for a Hydrogen-Fueled Recuperated 100 kW Class Gas Turbine. *J. Eng. Gas Turbines Power* **2017**, *139*, 082607, doi:10.1115/1.4035842.
74. Şahin, F.C. Experimental Investigation on Flow Improvement in Compressor Cascades. *Int. J. Energy Res.* **2017**, *41*, 526–539.
75. Gursul, I.; Cleaver, D.; Wang, Z. Control of Low Reynolds Number Flows by Means of Fluid-Structure Interactions. *Prog. Aerosp. Sci.* **2014**, *64*, 17–55.
76. Suman, A.; Fortini, A.; Aldi, N.; Pinelli, M.; Merlin, M. Analysis of the Aerodynamic and Structural Performance of a Cooling Fan With Morphing Blade. In Proceedings of the 12th European Conference on Turbomachinery Fluid Dynamics & Thermodynamics, Stockholm, Sweden, 3–7 April 2017.
77. Bilgen, O.; De Marqui, C., Jr.; Kochersberger, K.; Inman, D. Piezoceramic Composite Actuators for Flow Control in Low Reynolds Number Airflow. *J. Intell. Mater. Syst. Struct.* **2010**, *21*, 1201–1212.

78. Bilgen, O.; De Marqui, C., Jr.; Kochersberger, K.; Inman, D. Macro-Fiber Composite Actuators for Flow Control of a Variable Camber Airfoil. *J. Intell. Mater. Syst. Struct.* **2011**, *22*, 81–91.
79. Phan, T.D.; Springer, P.; Liebich, R. Numerical Investigation of an Elastomer-Piezo-Adaptive Blade for Active Flow Control of a Nonsteady Flow Field Using Fluid-Structure Interaction Simulations. *J. Turbomach.* **2017**, *139*, 091004, doi:10.1115/1.4036107.
80. Wang, J.; Li, Y.; Choi, K.S. Gurney Flap—Lift Enhancement, Mechanisms and Applications. *Prog. Aerosp. Sci.* **2008**, *44*, 22–47.
81. Feng, L.H.; Jukes, T.; Choi, K.S.; Wang, J.J. Flow Control over a NACA 0012 Airfoil Using Dielectric-Barrier-Discharge Plasma Actuator with a Gurney Flap. *Exp. Fluids* **2012**, *52*, 1533–1546.
82. Ismail, M.; Vijayaraghavan, K. The Effects of Aerofoil Profile Modification on a Vertical Axis Wind Turbine Performance. *Energy* **2015**, *80*, 20–31.
83. Lee, T.; Su, Y. Lift Enhancement and Flow Structure of Airfoil with Joint Trailing-Edge Flap and Gurney Flap. *Exp. Fluids* **2011**, *50*, 1671–1684.
84. Thamsen, P.; Hammer, S.; Peter, J.; Stiller, V. Gurney Flaps on Axial Pumps. In Proceedings of the 11th European Conference on Turbomachinery: Fluid Dynamics & Thermodynamics, Madrid, Spain, 23–27 March 2015.
85. Bechert, D.; Meyer, R.; Hage, W. Drag Reduction of Airfoils with Miniflaps. Can We Learn from Dragonflies? In Proceedings of the Fluids 2000 Conference and Exhibit, Denver, CO, USA, 19–22 June 2000.
86. Cole, J.; Vieira, B.; Coder, J.; Premi, A.; Maughmer, M. Experimental Investigation into the Effect of Gurney Flaps on Various Airfoils. *J. Aircr.* **2013**, *50*, 1287–1294.
87. Holst, D.; Pechlivanoglou, G.; Wegner, F.; Nayeri, C.; Paschereit, C. Potential of Retrofit Passive Flow Control for Small Horizontal Axis Wind Turbines. *J. Eng. Gas Turbines Power* **2017**, *139*, doi:10.1115/1.4034543.
88. Palacios, J.; Kinzel, M.; Overmeyer, A.; Szefi, J. Active Gurney Flaps: Their Application in a Rotor Blade Centrifugal Field. *J. Aircr.* **2014**, *51*, 473–489.
89. Dundi, T.; Sitaram, N.; Suresh, M. Application of Gurney Flaps on a Centrifugal Fan Impeller. *Int. J. Fluid Mach. Syst.* **2012**, *5*, 65–71.
90. Greenblatt, D. Application of Large Gurney Flaps on Low Reynolds Number Fan Blades. *J. Fluids Eng.* **2011**, *133*, 021102, doi:10.1115/1.4003301.
91. Lee, T. PIV Study of Near-Field Tip Vortex Behind Perforated Gurney Flaps. *Exp. Fluids* **2011**, *50*, 351–361.
92. Liu, L.; Padthe, A.; Friedmann, P. Computational Study of Microflaps with Application to Vibration Reduction in Helicopter Rotors. *AIAA J.* **2011**, *49*, 1450–1465.
93. Chen, P.P.; Qiao, W.Y.; Luo, H.L.; Hashmi, F. Investigation of Low Solidity LP Turbine Cascade with Flow Control: Part 1—Active Flow Control Using Jet-Flap. In Proceedings of the ASME Turbo Expo 2010: Power for Land, Sea, and Air, Glasgow, UK, 14–18 June 2010; Volume 7, pp. 1145–1154.
94. Chen, P.P.; Qiao, W.Y.; Luo, H.L. Investigation of Low Solidity LP Turbine Cascade With Flow Control: Part 2—Passive Flow Control Using Gurney-Flap. In Proceedings of the ASME Turbo Expo 2010: Power for Land, Sea, and Air, Glasgow, UK, 14–18 June 2010; Volume 7, pp. 1155–1162.
95. Traub, L.; Akerson, A. Airfoil Lift Augmentation at Low Reynolds Number. *J. Aircr.* **2010**, *47*, 2103–2114.
96. Byerley, A.; Störmer, O.; Baughn, J.; Simon, T.; Van Treuren, K.; List, J. Using Gurney Flaps to Control Laminar Separation on Linear Cascade Blades. *J. Turbomach.* **2003**, *125*, 114–120.
97. Martin, S.; Bhushan, B. Modeling and Optimization of Shark-Inspired Riblet Geometries for Low Drag Applications. *J. Colloid Interface Sci.* **2016**, *474*, 206–215.
98. Martin, S.; Bhushan, B. Discovery of Riblets in a Bird Beak (Rynchops) for Low Fluid Drag. *Philos. Trans. R. Soc. A* **2016**, *374*, 20160134, doi:10.1098/rsta.2016.0134.
99. Bechert, D.; Bruse, M.; Hage, W. Experiments with Three-Dimensional Riblets as an Idealized Model of Shark Skin. *Exp. Fluids* **2000**, *28*, 403–412.
100. Lee, S.J.; Lee, S.H. Flow Field Analysis of a Turbulent Boundary Layer over a Riblet Surface. *Exp. Fluids* **2001**, *30*, 153–166.
101. Nieuwstadt, F.; Wolthers, W.; Leijdens, H.; Krishna Prasad, K.; Schwarz-van Manen, A. The Reduction of Skin Friction by Riblets Under the Influence of an Adverse Pressure Gradient. *Exp. Fluids* **1993**, *15*, 17–26.
102. Bechert, D.W.; Bruse, M.; Hage, W.; Van der Hoeven, J.G.T.; Hoppe, G. Experiments on Drag-Reducing Surfaces and Their Optimization with an Adjustable Geometry. *J. Fluid Mech.* **1997**, *338*, 59–87.

103. Lietmeyer, C.; Denkena, B.; Krawczyk, T.; Klin, R.; Overmeyer, L.; Wojakowski, B.; Reithmeier, E.; Scheuer, R.; Vynnyk, T.; Seume, J. Recent Advances in Manufacturing of Riblets on Compressor Blades and Their Aerodynamic Impact. *J. Turbomach.* **2013**, *135*, 041008 doi:10.1115/1.4007590.
104. Viswanath, P. Aircraft Viscous Drag Reduction Using Riblets. *Prog. Aerosp. Sci.* **2002**, *38*, 571–600.
105. Debisschop, J.; Nieuwstadt, F. Turbulent Boundary Layer in an Adverse Pressure Gradient: Effectiveness of Riblets. *AIAA J.* **1996**, *34*, 932–937.
106. Truong, T.V.; Pulvin, P. Influence of Wall Riblets on Diffuser Flow. *Appl. Sci. Res.* **1989**, *46*, 217–227.
107. Squire, L.C.; Savill, A.M. Drag Measurements on Planar Riblet Surfaces at High Subsonic Speeds. *Appl. Sci. Res.* **1989**, *46*, 229–243.
108. Boomsma, A.; Sotiropoulos, F. Riblet Drag Reduction in Mild Adverse Pressure Gradients: A Numerical Investigation. *Int. J. Heat Fluid Flow* **2015**, *56*, 251–260.
109. Miao, X.; Zhang, Q.; Wang, L.; Jiang, H.; Qi, H. Application of Riblets on Turbine Blade Endwall Secondary Flow Control. *J. Propuls. Power* **2015**, *31*, 1578–1585.
110. Hergt, A.; Hage, W.; Grund, S.; Steinert, W.; Terhorst, M.; Schongen, F.; Wilke, Y. Riblet Application in Compressors: Towards Efficient Blade Design? In Proceedings of the ASME Turbo Expo 2014: Turbine Technical Conference and Exposition GT2014, Düsseldorf, Germany, 16–20 June 2014.
111. Chamorro, L.; Arndt, R.; Sotiropoulos, F. Drag Reduction of Large Wind Turbine Blades Through Riblets: Evaluation of Riblet Geometry and Application Strategies. *Renew. Energy* **2013**, *50*, 1095–1105.
112. Duan, L.; Choudhari, M.M. Effects of Riblets on Skin Friction in High Speed Turbulent Boundary Layers. In Proceedings of the 50th AIAA Aerospace Sciences Meeting including the New Horizons Forum and Aerospace Exposition, Nashville, TN, USA, 9–12 January 2012.
113. Sareen, A.; Deters, R.; Henry, S.; Selig, M. Drag Reduction Using Riblet Film Applied to Airfoils for Wind Turbines. In Proceedings of the 49th AIAA Aerospace Sciences Meeting including the New Horizons Forum and Aerospace Exposition, Orlando, FL, USA, 4–7 January 2011.
114. Klumpp, S.; Guldner, T.; Meinke, M.; Schröder, W. Riblets in a Turbulent Adverse-Pressure Gradient Boundary Layer. In Proceedings of the 5th Flow Control Conference, Chicago, IL, USA, 28 June–1 July 2010.
115. Gatti, D.; Quadrio, M. Reynolds-Number Dependence of Turbulent Skin-Friction Drag Reduction Induced by Spanwise Forcing. *J. Fluid Mech.* **2016**, *802*, 553–582.
116. Spalart, P.; Mclean, J. Drag Reduction: Enticing Turbulence, and Then an Industry. *Philos. Trans. R. Soc. A* **2011**, *369*, 1556–1569.
117. Lietmeyer, C.; Oehlert, K.; Seume, J. Optimal Application of Riblets on Compressor Blades and Their Contamination Behavior. In Proceedings of the ASME Turbo Expo 2011, Vancouver, BC, Canada, 6–10 June 2011.
118. Dean, B.; Bhushan, B. Shark-Skin Surfaces for Fluid-Drag Reduction in Turbulent Flow: A Review. *Philos. Trans. R. Soc. A* **2010**, *368*, 4775–4806.
119. García-Mayoral, R.; Jiménez, J. Drag Reduction by Riblets. *Philos. Trans. R. Soc. A* **2011**, *369*, 1412–1427.
120. Lee, S.J.; Choi, Y.S. Decrement of Spanwise Vortices by a Drag-Reducing Riblet Surface. *J. Turbul.* **2008**, *9*, 1–15.
121. Stenzel, V.; Wilke, Y.; Hage, W. Drag-Reducing Paints for the Reduction of Fuel Consumption in Aviation and Shipping. *Prog. Org. Coat.* **2011**, *70*, 224–229.
122. Schabowski, Z.; Hodson, H. The Reduction of Over Tip Leakage Loss in Unshrouded Axial Turbines Using Winglets and Squealers. *J. Turbomach.* **2014**, *136*, 041001, doi:10.1115/1.4024677.
123. Cheon, J.; Lee, S. Tip Leakage Aerodynamics over the Cavity Squealer Tip Equipped with Full Coverage Winglets in a Turbine Cascade. *Int. J. Heat Fluid Flow* **2015**, *56*, 60–70.
124. Han, S.; Zhong, J. Effect of Blade Tip Winglet on the Performance of a Highly Loaded Transonic Compressor Rotor. *Chin. J. Aeronaut.* **2016**, *29*, 653–661.
125. Jung, J.S.; Kwon, O.; Son, C. An Investigation on Aerodynamics Loss Mechanism of Squealer Tips of a High Pressure Turbine Blade Using URANS. In Proceedings of the ASME Turbo Expo 2016: Turbomachinery Technical Conference and Exposition, Seoul, South Korea, 13–17 June 2016; Volume 2D-2016.
126. Da Soghe, R.; Bianchini, C.; Toni, L.; Rubino, D. Effects of Impeller Squealer Tip on Centrifugal Compressor Performance. In Proceedings of the ASME Turbo Expo 2016: Turbomachinery Technical Conference and Exposition, Seoul, South Korea, 13–17 June 2016; Volume 2D-2016.

127. Caloni, S.; Shahpar, S.; Coull, J. Numerical Investigations of Different Tip Designs for Shroudless Turbine Blades. *Proc. Inst. Mech. Eng. Part A J. Power Energy* **2016**, *230*, 709–720.
128. Schabowski, Z.; Hodson, H.; Giacche, D.; Power, B.; Stokes, M. Aeromechanical Optimization of a Winglet-Squealer Tip for an Axial Turbine. *J. Turbomach.* **2014**, *136*, 071004, doi:10.1115/1.4025687.
129. Li, J.; Du, K.; Song, L. Effects of Tip Cavity Geometries on the Aerothermal Performance of the Transonic Turbine Blade with Cavity Tip. *Proc. Inst. Mech. Eng. Part A J. Power Energy* **2016**, *230*, 319–331.
130. Ma, H.; Wei, W.; Wang, L.; Tian, Y. Experimental Investigation of Effects of Suction-Side Squealer Tip Geometry on the Flow Field in a Large-Scale Axial Compressor using SPIV. *J. Therm. Sci.* **2015**, *24*, 303–312.
131. Came, P.M.; Robinson, C.J. Centrifugal Compressor Design. *Proc. Inst. Mech. Eng. Part C J. Mech. Eng. Sci.* **1999**, *213*, 139–155.
132. Chen, S.; Zhou, Z.; Meng, Q.; Wang, S.; Zhou, X. Experiment Study of the Winglet-Cavity Tip on the Aerodynamic Performance in a Turbine Cascade. *Proc. Inst. Mech. Eng. Part A J. Power Energy* **2017**, *231*, 676–685, doi:10.1177/0957650917720560.
133. Zhou, C.; Zhong, F. A Novel Suction-Side Winglet Design Philosophy for High-Pressure Turbine Rotor Tips. *J. Turbomach.* **2017**, *139*, 111002, doi:10.1115/1.4037056.
134. Lee, S.; Lee, S. Over-Tip Leakage Flow and Loss in a Turbine Cascade Equipped With Suction-Side Partial Squealers. *Int. J. Heat Fluid Flow* **2016**, *61*, 575–584.
135. Liu, Y.; Zhang, M.; Zhang, T.; Zhang, M.; He, Y. Effect of Winglet-Shroud Tip with Labyrinth Seals on Aerodynamic Performance of a Linear Turbine Cascade. *J. Fluids Eng. Trans. ASME* **2016**, *138*, 071103, doi:10.1115/1.4032752.
136. Liu, Y.; Zhang, T.L.; Zhang, M.; Zhang, M.C. Numerical and Experimental Investigation of Aerodynamic Performance for a Straight Turbine Cascade with a Novel Partial Shroud. *J. Fluids Eng. Trans. ASME* **2016**, *138*, 031206, doi:10.1115/1.4031556.
137. Zhou, K.; Zhou, C. Unsteady Aerodynamics of a Flat Tip and a Winglet Tip in a High-Pressure Turbine. In Proceedings of the ASME Turbo Expo 2016: Turbomachinery Technical Conference and Exposition, Seoul, South Korea, 13–17 June 2016; Volume 2D-2016.
138. Han, S.; Zhong, J.; Lu, H.; Kan, X.; Yang, L. Effect of Winglet Geometry Arrangement and Incidence on Tip Clearance Control in a Compressor Cascade. *J. Therm. Sci.* **2014**, *23*, 381–390.
139. Lee, S.; Lee, S. Tip Gap Flow Characteristics in a Turbine Cascade Equipped with Pressure-Side Partial Squealer Rims. *Int. J. Heat Fluid Flow* **2014**, *50*, 369–377.
140. Li, W.; Jiang, H.; Zhang, Q.; Lee, S. Squealer Tip Leakage Flow Characteristics in Transonic Condition. *J. Eng. Gas Turbines Power* **2014**, *136*, 042601, doi:10.1115/1.4025918.
141. Lee, S.; Kim, S.; Kim, K. Aerodynamic Performance of Winglets Covering the Tip Gap Inlet in a Turbine Cascade. *Int. J. Heat Fluid Flow* **2012**, *34*, 36–46.
142. Lee, S.; Chae, B. Effects of Squealer Rim Height on Aerodynamic Losses Downstream of a High-Turning Turbine Rotor Blade. *Exp. Therm. Fluid Science* **2008**, *32*, 1440–1447.
143. Prince, S.; Badalamenti, C.; Regas, C. The Application of Passive Air Jet Vortex-Generators to Stall Suppression on Wind Turbine Blades. *Wind Energy* **2017**, *20*, 109–123.
144. Baldacchino, D.; Manolesos, M.; Ferreira, C.; Gonzalez Salcedo, A.; Aparicio, M.; Chaviaropoulos, T.; Diakakis, K.; Florentie, L.; Garcia, N.; Papadakis, G.; et al. Experimental Benchmark and Code Validation for Airfoils Equipped With Passive Vortex Generators. *J. Phys.: Conf. Ser.* **2016**, *753*, 022002, doi:10.1088/1742-6596/753/2/022002.
145. Choudhry, A.; Arjomandi, M.; Kelso, R. Methods to Control Dynamic Stall for Wind Turbine Applications. *Renew. Energy* **2016**, *86*, 26–37.
146. Martinez Suarez, J.; Flaszynski, P.; Doerffer, P. Streamwise Vortex Generator for Separation Reduction on Wind Turbine Profile. *J. Phys.: Conf. Ser.* **2016**, *760*, 012018, doi:10.1088/1742-6596/760/1/012018.
147. Manolesos, M.; Voutsinas, S. Experimental Investigation of the Flow Past Passive Vortex Generators on an Airfoil Experiencing Three-Dimensional Separation. *J. Wind Eng. Ind. Aerodyn.* **2015**, *142*, 130–148.
148. Sitaram, N.; Swamy, S.M. Performance Improvement of a Centrifugal Compressor by Passive Means. *Int. J. Rotating Mach.* **2012**, 727259, doi:10.1155/2012/727259.
149. Lo, K.; Kontis, K. Flow Characteristics over a Tractor-Trailer Model with and without Vane-Type Vortex Generator Installed. *J. Wind Eng. Ind. Aerodyn.* **2016**, *159*, 110–122.

150. Bragin, N.; Ryabov, D.; Skomorokhov, S.; Slitinskaya, A. Study of Vortex Generator Influence on the Flow in the Wake of High-Lift System Wing. *AIP Conf. Proc.* **2016**, *1770*, 030032, doi:10.1063/1.4963974.
151. Tejero, F.; Doerffer, P.; Szulc, O. Application of a Passive Flow Control Device on Helicopter Rotor Blades. *J. Am. Helicopter Soc.* **2016**, *61*, 1–13.
152. Panaras, A.G.; Lu, F.K. Micro-Vortex Generators for Shock Wave/Boundary Layer Interactions. *Prog. Aerosp. Sci.* **2015**, *74*, 16–47.
153. Shan, H.; Jiang, L.; Liu, C.; Love, M.; Maines, B. Numerical Study of Passive and Active Flow Separation Control over a NACA0012 Airfoil. *Comput. Fluids* **2008**, *37*, 975–992.
154. Lin, J.C. Review of Research on Low-Profile Vortex Generators to Control Boundary-Layer Separation. *Prog. Aerosp. Sci.* **2002**, *38*, 389–420.
155. Zhao, Y.; Lu, H.; Sun, Y. Experimental Studies of Dimpled Surface Effect on the Performance of Linear Cascade under Different Incidence Angles. *Procedia CIRP* **2016**, *56*, 137–142.
156. Tay, C.; Khoo, B.; Chew, Y. Mechanics of Drag Reduction by Shallow Dimples in Channel Flow. *Phys. Fluids* **2015**, *27*, 035109, doi:10.1063/1.4915069.
157. Murata, A.; Yano, K.; Hanai, M.; Saito, H.; Iwamoto, K. Arrangement Effects of Inclined Teardrop-Shaped Dimples on Film Cooling Performance of Dimpled Cutback Surface at Airfoil Trailing Edge. *Int. J. Heat Mass Transf.* **2017**, *107*, 761–770.
158. Ligrani, P. Heat Transfer Augmentation Technologies for Internal Cooling of Turbine Components of Gas Turbine Engines. *Int. J. Rotating Mach.* **2013**, 275653, doi:10.1155/2013/275653.
159. Gupta, S.; Chaube, A.; Verma, P. Review on Heat Transfer Augmentation Techniques: Application in Gas Turbine Blade Internal Cooling. *J. Eng. Sci. Technol. Rev.* **2012**, *5*, 57–62.
160. Dees, J.; Bogard, D.; Bunker, R. Heat Transfer Augmentation Downstream of Rows of Various Dimple Geometries on the Suction Side of a Gas Turbine Airfoil. *J. Turbomach.* **2010**, *132*, 031010, doi:10.1115/1.3149284.
161. Whitfield, A.; Abdullah, A. The Performance of a Centrifugal Compressor with High Inlet Prew whirl. *J. Turbomach.* **1998**, *120*, 487–493.
162. Galindo, J.; Serrano, J.; Margot, X.; Tiseira, A.; Schorn, N.; Kindl, H. Potential of Flow Pre-Whirl at the Compressor Inlet of Automotive Engine Turbochargers to Enlarge Surge Margin and Overcome Packaging Limitations. *Int. J. Heat Fluid Flow* **2007**, *28*, 374–387.
163. Guendogdu, Y.; Vorreiter, A.; Seume, J. Design of a Low Solidity Flow-Controlled Stator with Coanda Surface in a High Speed Compressor. In Proceedings of the ASME Turbo Expo 2008: Power for Land, Sea, and Air, Berlin, Germany, 9–13 June 2008; Volume 6, pp. 629–639.
164. Fouatih, O.; Medale, M.; Imine, O.; Imine, B. Design Optimization of the Aerodynamic Passive Flow Control on NACA 4415 Airfoil Using Vortex Generators. *Eur. J. Mech. B. Fluids* **2016**, *56*, 82–96.
165. Zhou, W.; Rao, Y.; Hu, H. An Experimental Investigation on the Characteristics of Turbulent Boundary Layer Flows over a Dimpled Surface. *J. Fluids Eng. Trans. ASME* **2016**, *138*, 021204, doi:10.1115/1.4031260.
166. Miller, E. Effects on Boundary Layer Caused by Inclusion of Dimples at Varying Depths. *J. Aircr.* **2012**, *49*, 969–972.
167. Shahpar, S.; Caloni, S.; de Prieëlle, L. Automatic Design Optimization of Profiled Endwalls Including Real Geometrical Effects to Minimize Turbine Secondary Flows. *J. Turbomach.* **2017**, *139*, 071010, doi:10.1115/1.4035510.
168. Zaryankin, A.; Rogalev, A.; Kindra, V.; Khudyakova, V.; Bychkov, N. Reduction Methods of Secondary Flow Losses in Stator Blades: Numerical and Experimental Study. In Proceedings of the 12th European Conference on Turbomachinery Fluid Dynamics & Thermodynamics, Stockholm, Sweden, 3–7 April 2017.
169. Bareiß, S.; Vogt, D.M.; Chebli, E. Investigation on the Impact of Circumferential Grooves on Aerodynamic Centrifugal Compressor Performance. In Proceedings of the ASME Turbo Expo 2015: Turbine Technical Conference and Exposition, Montreal, QC, Canada, 15–19 June 2015.
170. Wang, W.; Chu, W.; Zhang, H.; Wu, Y. Experimental Study of Self-Recirculating Casing Treatment in a Subsonic Axial Flow Compressor. *Proc. Inst. Mech. Eng. Part A J. Power Energy* **2016**, *230*, 805–818.
171. Jung, S.; Pelton, R. Numerically Derived Design Guidelines of Self Recirculation Casing Treatment for Industrial Centrifugal Compressors. In Proceedings of the ASME Turbo Expo 2016: Turbomachinery Technical Conference and Exposition, Seoul, South Korea, 13–17 June 2016; Volume 2D-2016.

172. Tun, M.; Sakaguchi, D. Multi-point Optimization of Recirculation Flow Type Casing Treatment in Centrifugal Compressors. *J. Therm. Sci.* **2016**, *25*, 231–241.
173. Zheng, X.; Zhang, Y.; Yang, M.; Bamba, T.; Tamaki, H. Stability Improvement of High-Pressure-Ratio Turbocharger Centrifugal Compressor by Asymmetrical Flow Control-Part II: Nonaxisymmetrical Self-Recirculation Casing Treatment. *J. Turbomach.* **2012**, *135*, 021007, doi:10.1115/1.4006637.
174. Zhu, M.; Qiang, X.; Yu, W.; Teng, J. Analysis on Slot-Type Casing Treatment Injection Flow in an Axial Transonic Compressor. *Proc. Inst. Mech. Eng. Part A* **2016**, *230*, 792–804.
175. Irsch, M.P.; Davis, R.; Paniagua, G.; Clark, J. Flow Control of Unsteadiness in the Wake of a Turbine Blade. In Proceedings of the 53rd AIAA Aerospace Sciences Meeting, Kissimmee, FL, USA, 5–9 January 2015.
176. Nie, C.; Tong, Z.; Geng, S.; Zhu, J.; Huang, W. Experimental Investigations of Micro Air Injection to Control Rotating Stall. *J. Therm. Sci.* **2007**, *16*, 1–6.
177. Wang, T.; Xu, W.; Gu, C.; Xiao, J. A New Type of Self-Adaptive Casing Treatment for a Centrifugal Compressor. In Proceedings of the ASME Turbo Expo 2010: Power for Land, Sea and Air, Glasgow, UK, 14–18 June 2010; Volume 7, pp. 2065–2074.
178. Skoch, G. Experimental Investigation of Centrifugal Compressor Stabilization Techniques. *J. Turbomach.* **2003**, *125*, 704–713.
179. Azzam, T.; Paridaens, R.; Ravelet, F.; Khelladi, S.; Oualli, H.; Bakir, F. Experimental Investigation of an Actively Controlled Automotive Cooling Fan Using Steady Air Injection in the Leakage Gap. *Proc. Inst. Mech. Eng. Part A* **2017**, *231*, 56–67.
180. Christou, G.A.; Tan, C.S.; Sirakov, B.T.; Lei, V.M.; Alescio, G. Characterizing Flow Effects of Ported Shroud Casing Treatment on Centrifugal Compressor Performance. *J. Turbomach.* **2017**, *139*, 081005, doi:10.1115/1.4035664.
181. Du, J.; Seume, J.R. Design of Casing Treatment on a Mixed-Flow Compressor. In Proceedings of the ASME Turbo Expo 2017: Turbomachinery Technical Conference and Exposition, Charlotte, NC, USA, 26–30 June 2017.
182. Guinet, C.; Inzenhofer, A.; Gümmer, V. Influencing Parameters of Tip Blowing Interacting with Rotor Tip Flow. *J. Turbomach.* **2017**, *139*, 021010, doi:10.1115/1.4034699.
183. Hirano, T.; Ogawa, T.; Yasui, R.; Tsujita, H. Effect of Double Air Injection on Performance Characteristics of Centrifugal Compressor. *J. Therm. Sci.* **2017**, *26*, 11–17.
184. Kern, F.; Brehm, S.; Niehuis, R. Ejector Tip Injection System for Active Aerodynamic Compressor Stabilization Part I: Design and Experiment. In Proceedings of the 12th European Conference on Turbomachinery Fluid Dynamics & Thermodynamics, Stockholm, Sweden, 3–7 April 2017.
185. Senel, C.; Maral, H.; Kavurmacioglu, L.A.; Camci, C. An Investigation of Groove Type Casing Treatment on Aerodynamic Performance of a Linear Turbine Cascade. In Proceedings of the 12th European Conference on Turbomachinery Fluid Dynamics & Thermodynamics, Stockholm, Sweden, 3–7 April 2017.
186. Volino, R.J. Control of Tip Leakage in a High-Pressure Turbine Cascade Using Tip Blowing. *J. Turbomach.* **2017**, *139*, 061008, doi:10.1115/1.4035509.
187. Cevik, M.; Vo, H.; Yu, H. Casing Treatment for Desensitization of Compressor Performance and Stability to Tip Clearance. *J. Turbomach.* **2016**, *138*, 121008, doi:10.1115/1.4033420.
188. DeGroot, C.; Wang, C.; Floryan, J. Drag Reduction Due to Streamwise Grooves in Turbulent Channel Flow. *J. Fluids Eng. Trans. ASME* **2016**, *138*, 121201, doi:10.1115/1.4034098.
189. Li, J.; Du, J.; Nan, X.; Liu, L.; Lin, F. Coupling Stability-Enhancing Mechanism with Compact Self-Recirculating Injection in an Axial Flow Compressor. *Proc. Inst. Mech. Eng. Part A* **2016**, *230*, 696–708.
190. Liu, L.; Li, J.; Nan, X.; Lin, F. The Stall Inceptions in an Axial Compressor with Single Circumferential Groove Casing Treatment at Different Axial Locations. *Aerosp. Sci. Technol.* **2016**, *59*, 145–154.
191. Sun, D.; Nie, C.; Liu, X.; Lin, F.; Sun, X. Further Investigation on Transonic Compressor Stall Margin Enhancement with Stall Precursor-Suppressed Casing Treatment. *J. Turbomach.* **2016**, *138*, 021001, doi:10.1115/1.4031775.
192. Halawa, T.; Gadala, M.S.; Alqaradawi, M.; Badr, O. Optimization of the Efficiency of Stall Control Using Air Injection for Centrifugal Compressors. *J. Eng. Gas Turbines Power* **2015**, *137*, 072604, doi:10.1115/1.4029169.
193. Hirano, T.; Takano, M.; Tsujita, H. Effect of Double Air Injection on Performance Characteristics of Centrifugal Compressor. *J. Therm. Sci.* **2015**, *24*, 10–16.

194. Wang, W.; Chu, W.; Zhang, H. Numerical Investigation on the Effect of a Plenum Chamber with Slot-Type Casing Treatment on the Performance of an Axial Transonic Compressor. *Proc. Inst. Mech. Eng. Part A* **2015**, *229*, 393–405.
195. Ding, L.; Wang, T.; Yang, B.; Xu, W.; Gu, C. Experimental Investigation of the Casing Treatment Effects on Steady and Transient Characteristics in an Industrial Centrifugal Compressor. *Exp. Therm. Fluid Sci.* **2013**, *45*, 136–145.
196. Hu, L.; Sun, H.; Yi, J.; Curtis, E.; Zhang, J.; Yang, C.; Krivitziky, E. Numerical and Experimental Investigation of a Compressor with Active Self-Recirculation Casing Treatment for a Wide Operation Range. *Proc. Inst. Mech. Eng. Part D* **2013**, *227*, 1227–1241.
197. Sivagnanasundaram, S.; Spence, S.; Early, J.; Nikpour, B. An Impact of Various Shroud Bleed Slot Configurations and Cavity Vanes on Compressor Map Width and the Inducer Flow Field. *J. Turbomach.* **2013**, *135*, 041003, doi:10.1115/1.4007513.
198. Tamaki, H. Effect of Recirculation Device with Counter Swirl Vane on Performance of High Pressure Ratio Centrifugal Compressor. *J. Turbomach.* **2012**, *134*, 051036, doi:10.1115/1.4004820.
199. Xu, W.; Wang, T.; Gu, C.; Ding, L. A Study on the Influence of Hole's Diameter With Holed Casing Treatment. In Proceedings of the ASME Turbo Expo 2011, Vancouver, BC, Canada, 6–10 June 2011; Volume 4, pp. 499–508.
200. Hirano, T.; Uchida, T.; Tsujita, H. Control of Surge in Centrifugal Compressor by Using a Nozzle Injection System: Universality in Optimal Position of Injection Nozzle. *Int. J. Rotating Mach.* **2012**, 259293, doi:10.1155/2012/259293.
201. Skoch, G. Experimental Investigation of Diffuser Hub Injection to Improve Centrifugal Compressor Stability. *J. Turbomach.* **2005**, *127*, 107–117.
202. Spakovszky, Z. Backward Traveling Rotating Stall Waves in Centrifugal Compressors. *J. Turbomach.* **2004**, *126*, 1–12.
203. Spakovszky, Z.; Roduner, C. Spike and Modal Stall Inception in an Advanced Turbocharger Centrifugal Compressor. *J. Turbomach.* **2009**, *131*, 031012, doi:10.1115/1.2988166.
204. Japikse, D. *Turbomachinery Diffuser Design Technology*; Concepts ETI: Norwich, UK, 1984.
205. Jones, B.A. Centrifugal Compressor Boundary Layer Control. U.S. Patent 3,893,787, 8 July 1975.



© 2017 by the authors. Licensee MDPI, Basel, Switzerland. This article is an open access article distributed under the terms and conditions of the Creative Commons Attribution NonCommercial NoDerivatives (CC BY-NC-ND) license (<https://creativecommons.org/licenses/by-nc-nd/4.0/>).